NASA TECHNICAL NOTE

NASA TN D-2236

NASA TN D-2236

EFFECTS OF SPANWISE VARIATION OF LEADING-EDGE SWEEP ON THE LIFT, DRAG, AND PITCHING MOMENT OF A WING-BODY COMBINATION AT MACH NUMBERS FROM 0.7 TO 2.94

by Raymond M. Hicks and Edward J. Hopkins

Ames Research Center
Moffett Field, Calif.

NATIONAL AERONAUTICS AND SPACE ADMINISTRATION • WASHINGTON, D. C. • APRIL 1964

EFFECTS OF SPANWISE VARIATION OF LEADING-EDGE SWEEP ON THE LIFT, DRAG, AND PITCHING MOMENT OF A WING-BODY COMBINATION AT MACH NUMBERS FROM 0.7 TO 2.94

By Raymond M. Hicks and Edward J. Hopkins

Ames Research Center
Moffett Field, Calif.

NATIONAL AERONAUTICS AND SPACE ADMINISTRATION

For sale by the Office of Technical Services, Department of Commerce,
Washington, D.C. 20230 -- Price $1.50

EFFECTS OF SPANWISE VARIATION OF LEADING-EDGE SWEEP ON THE LIFT, DRAG, AND PITCHING MOMENT OF A WING-BODY COMBINATION AT MACH NUMBERS FROM 0.7 TO 2.94

By Raymond M. Hicks and Edward J. Hopkins

Ames Research Center
Moffett Field, Calif.

SUMMARY

Lift, drag, and pitching-moment characteristics of four wing-body combinations are presented. Two of the wings were used for reference and had straight leading edges, one of triangular plan form and the other of trapezoidal plan form. The other two wings were modifications of the reference plan forms. The modified trapezoidal plan form had a gradual reduction in sweep from a highly swept inboard portion of the span to a moderate sweep at the tip. The modified triangular plan form had high sweep over the inboard portion of the span, moderate sweep near the center of the span, and high sweep at the tip, thereby forming an ogee plan form. All wings had the same trailing-edge sweep, thickness ratio, exposed area, exposed span, and, hence, exposed aspect ratio. The wings were mounted alternately on a cylindrical body and were sufficiently far aft to be out of the region of pressure gradients emanating from the Sears-Haack nose. Results of this investigation are presented throughout a Mach number range from 0.7 to 2.94 at a constant unit Reynolds number of 2.5 million per foot. Experimental forces and moments are compared with the predicted values for the plan forms with straight leading edges.

The maximum lift-drag ratios of the various wings are compared on the basis of an all-turbulent boundary layer and zero leading-edge thickness throughout the Mach number range of the investigation. Sublimation pictures were used to adjust the basic data to the condition corresponding to an all-turbulent boundary layer.

The results of this investigation show that at all supersonic Mach numbers above 1.4, the ogee plan form had the highest maximum lift-drag ratio, but at subsonic Mach numbers the modified trapezoidal plan form had the highest aerodynamic efficiency. The nonlinear variation of pitching moment with lift exhibited by the trapezoidal plan form at transonic Mach numbers did not occur for the modified trapezoidal plan form.

INTRODUCTION

According to linear, nonviscous, supersonic theory (e.g., refs. 1 and 2), the most efficient flight at supersonic speeds should be realized by high-aspect-ratio arrow wings with subsonic leading edges. In wind-tunnel

experiments, however, these theoretically ideal wings do not attain their predicted high aerodynamic efficiencies because in a real viscous fluid the boundary layer drains toward the wing tip and precipitates leading-edge-flow separation which prevents the realization of the predicted leading-edge thrust (see ref. 3). At low subsonic speeds high-aspect-ratio arrow wings exhibit undesirable pitch-up tendencies associated with the flow separation at their wing tips. One method of alleviating these pitch-up tendencies is to shorten the wing span or reduce the aspect ratio until the plan form is nearly triangular. Such a plan-form modification will lead to high induced drag and inefficient flight at subsonic speeds. A possible solution to the problem of attaining efficient flight at both subsonic and supersonic speeds involves the use of variable-sweep wings whereby the leading-edge sweep is decreased as the flight speed is reduced. This solution has several basic disadvantages, namely, increased weight, increased complexity, and decreased reliability.

The present experimental investigation was undertaken to explore the possibility of improving the aerodynamic characteristics of low-aspect-ratio wings of fixed geometry at both low and high speeds by varying the leading-edge sweep over the span. To accomplish this leading-edge sweep variation without any abrupt changes in the leading edge, two wings with curved leading edges were designed and tested, one with an ogee plan form and the other with a modified trapezoidal plan form. An average leading-edge sweep for these wings was chosen so that, in general, the combination of this sweep angle and the aspect ratio would, according to reference 4, result in a nearly linear pitching-moment curve at low speeds. To evaluate the effects of leading-edge curvature on the lift, drag, and pitching moments, two other wings with triangular and trapezoidal plan forms having straight leading edges were also investigated throughout a Mach number range from 0.7 to 2.94. All four wings were designed to have the same exposed aspect ratio, area, average exposed chord, trailing-edge sweep, and thickness ratio. Experimental results for the two wings with straight leading edges are compared with results predicted from linear theory.

NOTATION

C_D' drag coefficient uncorrected to zero leading-edge thickness or to an all-turbulent boundary layer, $\frac{\text{drag (measured)}}{qS}$

C_D drag coefficient corrected to zero leading-edge thickness and to an all-turbulent boundary layer, $\frac{\text{drag (corrected)}}{qS}$

C_{D_o} minimum drag coefficient obtained from an extrapolation of the drag due to lift curve to zero lift coefficient after corrections were applied for zero leading-edge thickness and for an all-turbulent boundary layer

C_L lift coefficient, $\frac{\text{lift}}{qS}$

C_m pitching-moment coefficient, $\frac{\text{pitching moment about moment centers shown in figure 1}}{qS\bar{c}}$

$\frac{\partial C_L}{\partial \alpha}$ lift-curve slope measured at $\alpha = 0^\circ$

$\frac{\partial C_D}{\partial C_L^2}$ drag-rise factor

$\left(\frac{L}{D}\right)_{max}$ maximum ratio of lift to corrected drag, $\frac{C_L}{C_D}$

$\frac{\partial C_m}{\partial C_L}$ pitching-moment-curve slope measured at $C_L = 0$

α angle of attack

b wing span

c local wing chord for triangular wing

$\bar{c}$ mean aerodynamic chord of triangular wing

M Mach number

q free-stream dynamic pressure

r body radius

$\frac{R}{l}$ free-stream unit Reynolds number

S wing area of triangular wing including area blanketed by the body

y lateral distance as defined in figure 1

MODEL DESCRIPTION

The wings selected for this investigation were an ogee wing, a modified trapezoidal wing, a triangular wing, and a trapezoidal wing. Dimensional data for each of these wings are shown in figure 1. Photographs of the wing-body combinations are shown in figure 2. All wings had an exposed aspect ratio of 2.17, a hexagonal airfoil section, with a constant thickness of 2 percent of the local chord from 30- to 70-percent chord, an exposed average chord of 2.761 inches, a trailing edge swept forward 10°, and a span of 6.875 inches. Each wing was mounted in the horizontal plane of symmetry on a body of revolution which had a Sears-Haack nose and a cylindrical afterbody. All models were constructed of solid steel.

For the purpose of estimating the drag associated with the finite leading-edge thickness required for wind-tunnel models, the following average thicknesses were measured on a profilometer with a magnification of X100.

Wing	Leading-edge thickness, in.
Ogee	0.007
Modified trapezoidal	.007
Triangular	.007
Trapezoidal	.009

TEST PROCEDURE

The tests were conducted at Mach numbers of 0.7, 0.9, 1.0, 1.1, and 1.4 in the Ames 2- by 2-foot transonic wind tunnel and 1.98 and 2.94 in the Ames 1- by 3-foot supersonic wind tunnel. The unit Reynolds number was held constant at 2.5 million per foot; therefore the Reynolds number based on the average exposed chord was 0.58 million for all models. Data were taken at angles of attack -4°, -3°, -2°, -1°, 0°, 1°, 2°, 3°, 4°, 6°, and 8° at each Mach number. The first part of this test was devoted to investigating the possibility of fixing transition at the leading edge of the wing by one row of three-dimensional roughness elements placed about 1/8 inch behind the leading edge. Because of the high Mach number, low Reynolds number, and small model size, a 25-percent increase in drag above the value for an all-turbulent boundary layer was incurred by use of these elements. The incremental drag due to the roughness was determined by testing roughness elements several sizes larger than that necessary to fix transition. Because of the inherent inaccuracies in the method, it was believed that the results of the test would be more reliable if the data were obtained with natural transition.

In order to adjust the drag data taken with natural transition to conditions corresponding to an all-turbulent boundary layer, it is necessary to know where transition occurs on the surfaces. The location of boundary-layer transition was determined by sublimation photographs taken at angles of attack of 0° and 4°.

REDUCTION OF DATA

Corrections

The measured axial force used in the computation of the drag coefficients was adjusted so that the base pressure of the model was equal to the free-stream static pressure. The angle of attack was corrected for sting and balance deflections caused by the normal force and pitching moment, and C_L, C_D, and C_m were corrected for interactions between the various components of the balance.

At an angle of attack of 0° all surfaces had a nearly all-laminar boundary layer. Since this was not typical of the flow conditions at the higher angles of attack, the sublimation data taken at $\alpha = 4^\circ$ (the approximate angle of attack for maximum lift-drag ratio for all the wings) were used to adjust the drag data to conditions for an all-turbulent boundary layer. The method used for making this correction is presented in appendix A.

To preserve a smooth leading edge free of imperfections which promote premature transition locally, the models were constructed with a slight leading-edge bluntness. The wind-tunnel data must be corrected for the drag increment associated with this leading-edge bluntness, since a full-sized wing will have a much sharper leading edge relatively than a model of this scale. The method used for making this correction is presented in appendix B.

The corrections which were applied for not having an all-turbulent boundary layer and for zero leading-edge thickness are listed in table I. These skin-friction and bluntness drag corrections were applied only to the data given in the summary figures 12 and 13. The basic force data presented in figures 3 to 9 have not been adjusted for these corrections.

Accuracy

The accuracy of the data listed below is based on the repeatability and known precision of the measuring equipment.

C_L	± 0.002
C_m	± 0.004
C_D	± 0.0002
α	$\pm 0.05^\circ$
M	± 0.01
R	$\pm 0.01 \times 10^6$

THEORETICAL METHODS OF ANALYSIS

Lift and Pitching Moments

Interference effects.- The method of reference 5, which includes the mutual interference effects between the wing and the body, was used to estimate the lift and pitching moments of the body in combination with either the triangular wing or the trapezoidal wing. No similar calculations were made for the wings with curved leading edges for lack of proven theoretical methods. The adequacy of reference 5 in predicting the lift and the pitching moments of wing-body combinations depends directly on how accurately the wing alone and body alone characteristics can be predicted.

Wing alone.- At subsonic speeds each of two different methods, that of Lomax (ref. 6) and that of Weissinger (ref. 7), was employed to estimate the lift and pitching moments for both the triangular and trapezoidal plan forms. At supersonic speeds the lift for both of these plan forms was estimated by linear theory from the charts presented in reference 8 for the triangular plan form and from the charts presented in reference 9 for the trapezoidal plan form. The aerodynamic centers at supersonic speeds were taken from reference 5.

Body alone.- The lift and pitching moments for the body were estimated throughout the Mach number range from the slender-body concepts presented in reference 5. No viscous cross forces were taken into account.

Drag

Wave drag.- At zero lift the wave drag was calculated by application of the supersonic area rule on a digital computer. For the calculation, an "equivalent" body of revolution of the wing and body was obtained for each family of parallel oblique cutting planes. The wave drag was computed from these area distributions by an integration process as given by the Von Kármán wave-drag formula for a slender body of revolution as applied by Jones (ref. 10) and others for arbitrary configurations at supersonic speeds. No angle-of-attack effect on wave drag was considered.

Skin-friction drag.- A complete description of the method used for computing the skin-friction drag is presented in appendix A. Each wing-body combination was treated as a flat plate with no additional corrections being applied for mutual interference effects between surfaces or for the shear layer induced by slight leading-edge bluntness.

Drag due to lift.- Since all wings had sharp leading edges, no leading-edge thrust would be expected; therefore, the drag due to lift was assumed to be equal to the lift times the angle of attack.

Maximum lift-drag ratio.- In accordance with the above assumptions a parabolic drag polar was assumed, so that the maximum lift-drag ratio for an uncambered wing is defined as

$$\left(\frac{L}{D}\right)_{max} = \frac{1}{2}\sqrt{\frac{C_{L_\alpha}}{C_{D_o}}} \tag{1}$$

RESULTS AND DISCUSSION

Presentation of Results

The lift, drag, pitching moment and drag due to lift are presented in figures 3 to 9, inclusive.[1] The maximum lift-drag ratios, minimum drag coefficients, lift-curve slopes, drag-rise factors, and pitching-moment curve slopes obtained from the data of figures 3 through 9 are summarized in figures 10 through 14. The summary plots of minimum drag coefficient and maximum lift-drag ratio are presented for an all-turbulent boundary layer and zero leading-edge bluntness (see appendixes A and B and table I for the methods and drag increments used for correcting the data presented in figures 12 and 13). The predicted values of the above parameters for the triangular and trapezoidal wings are shown also on the summary plots.

Discussion of Experimental Results

The drag polars and drag-due-to-lift curves generally show a large decrease in drag near zero angle of attack. This can be attributed to an increased amount of laminar flow over the upper surface of the wings as indicated by the sublimation photographs shown in figure 15. It was found that near the angle of attack for maximum lift-drag ratio ($\alpha \approx 4^\circ$) there was little movement of transition on either the wings or the body as the model was pitched through a small angle-of-attack range. Hence, the drag-due-to-lift curves at the higher lift coefficients have been extrapolated to zero lift coefficient as indicated by the dashed curves (figs. 3(b) through 9(b)). The corresponding values of minimum drag coefficient (C_{D_o}) corrected to zero leading-edge thickness and to the condition of an all-turbulent boundary layer are presented in the summary curves (fig. 12). These derived values of minimum drag coefficient were used to obtain the corrected values of maximum lift-drag ratio shown in figure 13. Polars show dashed extrapolations near zero lift coefficient corresponding to the extrapolations shown on the drag-due-to-lift curves (figs. 3(a) through 9(a)).

At subsonic Mach numbers the modified trapezoidal wing had the highest maximum lift-drag ratio reaching a maximum value of 8.4 at a Mach number of 0.90

[1]These results are not modified to the condition of zero leading-edge bluntness and an all-turbulent boundary layer.

(see fig. 13). This result is traceable to the modified trapezoidal wing having the lowest drag due to lift and relatively low minimum drag. The ogee wing had maximum lift-drag ratios only slightly below those for the modified trapezoidal wing at these Mach numbers. At Mach numbers of 1.0, 1.1, and 1.4 the ogee and the modified trapezoidal wings had higher maximum lift-drag ratios than either the triangular or trapezoidal wings. The decrease in maximum lift-drag ratio with Mach number was less for the ogee wing than the other wings as the Mach number was increased above 1.4. This resulted in a maximum lift-drag ratio which was about 0.5 higher than for any other wings tested at a Mach number of 2.94 (see fig. 13). The higher maximum lift-drag ratio is attributed to the unexplained lower minimum drag coefficient for the ogee wing.

The range of the aerodynamic center movement (in percent of the mean aerodynamic chord of the triangular wing) with Mach number was approximately the same for the triangular, ogee, and modified trapezoidal wings. The trapezoidal wing (see fig. 14) exhibited the largest shift in aerodynamic center at transonic speeds. It is interesting to note that this large shift was reduced by the increased sweep of the leading-edge extension near the root of the modified trapezoidal wing. This leading-edge extension near the wing root also tended to eliminate the nonlinear character of the pitching-moment curves of the trapezoidal wing at transonic Mach numbers (see figs. 3(a) through 6(a)).

Comparison With Theory

At subsonic and transonic speeds the Weissinger-Nielsen method gave the best estimate of lift-curve slope, drag due to lift, maximum lift-drag ratio, and pitching-moment curve slope for the trapezoidal wing, whereas the Lomax-Nielsen method gave the best estimate for the triangular wing (see figs. 10(b), 11(b), 13(b), and 14(b)).

At supersonic speeds the Eichelbrenner-Nielsen method showed good agreement with experiment for the triangular wing whereas the Lagerstrom-Nielsen method showed good agreement with experiment for the trapezoidal wing (see figs. 10(b), 11(b), 13(b), and 14(b)).

The agreement between the experimental drag due to lift and the reciprocal of the experimental lift-curve slope is better for the plan forms with curved leading edges than for those with straight leading edges as shown in figure 11.

At subsonic Mach numbers the predicted values of minimum drag coefficient agreed very well with those from experiment for the triangular and ogee wings (see fig. 12). However, the predicted values were slightly lower than the experimental values for the modified trapezoidal wing and considerably lower than experiment for the trapezoidal wing. It is possible that part of this disagreement between experiment and theory can be attributed to compressibility effects. At $M = 1.0$ predicted values were higher than experimental values for all wings as a result of the extremely high theoretical values of wave drag. At a Mach number of 2.94 the theoretical values of minimum drag coefficient were less than the experimental values except for the ogee wing which had the

lowest measured drag. Because of a less efficient surface area distribution the predicted value of C_{D_o} for the trapezoidal wing is about 5 percent higher than that for the triangular wing at $M = 2.94$ even though both wings have the same average chords.

SUMMARY OF RESULTS

Experimental measurements and some theoretical estimates have been made of the lift, drag, and pitching-moment characteristics of four wing-body combinations over a Mach number range from 0.7 to 2.94. The four wings of equal span, area, and thickness-to-chord ratio had an aspect ratio of 2.17 and included triangular, ogee, trapezoidal, and modified trapezoidal plan forms.

This investigation has shown that small gains in the aerodynamic efficiency of a triangular wing and a trapezoidal wing can be attained throughout a Mach number range from 0.7 to 2.94 by the use of spanwise variation of leading-edge sweep.

At subsonic and low supersonic Mach numbers the nonlinearity of the pitching-moment curve exhibited by the trapezoidal wing was eliminated by the increased sweep of the leading edge near the root of the modified trapezoidal wing.

The theoretical Lomax-Nielsen method gave a better prediction of the aerodynamic characteristics of the triangular wing than the Weissinger-Nielsen method at subsonic Mach numbers whereas the opposite was true for the trapezoidal wing. In general, the maximum lift-drag ratio of the triangular and trapezoidal wings was adequately predicted at supersonic Mach numbers. At a Mach number of 2.94 the theoretical minimum drag coefficients were lower than the experimental values except for the ogee wing which had the lowest drag.

Ames Research Center
National Aeronautics and Space Administration
Moffett Field, Calif., Jan. 8, 1964

APPENDIX A

SKIN-FRICTION DRAG CALCULATIONS

As pointed out in Test Procedure, no boundary-layer trip was employed because of the large drag increment which would result particularly at the high Mach numbers. Instead the drag data obtained with natural transition were corrected to conditions corresponding to those in which an all-turbulent boundary layer occurred at the wind-tunnel Reynolds number.[1] The method used for making this correction is presented below. To establish where boundary-layer transition occurred, sublimation photographs were taken throughout the test Mach number range of all model surfaces with the model at an angle of attack of 4°, the approximate angle of attack for maximum lift-to-drag ratio. Typical photographs for each model at a Mach number of 2.94 are presented in figure 16. The first step in the calculations was that of measuring the amount of chordwise laminar flow at several spanwise stations on each model. In general, measurements were made at 5 to 10 spanwise stations, depending upon the complexity of the flow pattern. To determine the skin friction at each spanwise station where the boundary layer was both laminar and turbulent, the measured distance for laminar flow was transformed into an equivalent distance for turbulent flow. This equivalent distance is shown as x_V in the sketch.

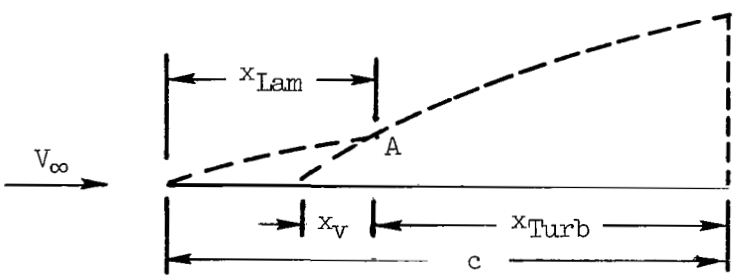

Justification for using x_V in the calculations is that the momentum losses in the boundary layer at point A associated with the laminar boundary layer ahead of point A can be considered to be the same as those for a turbulent boundary layer acting over a shorter distance, x_V, ahead of point A. This distance to the virtual origin of turbulent flow was found by equating the turbulent skin-friction drag given by Von Kármán's power function equation in reference 11 to the laminar skin-friction drag given by the Blasius equation, both equations being corrected for compressibility effects. This equivalence equation can be written as

$$\frac{0.074(x_V)^{0.8}}{(R/l)^{0.2}}\left(\frac{C_f}{C_{f_i}}\right)_{Turb} = \frac{1.327\sqrt{x_{Lam}}}{(R/l)^{0.5}}\left(\frac{C_f}{C_{f_i}}\right)_{Lam} \qquad (A1)$$

[1]Only the maximum lift-drag ratios and the minimum drag coefficients presented in figures 12 and 13 have been corrected in this manner.

when the compressibility factors were approximated for an adiabatic flat plate as

$$\left(\frac{C_f}{C_{f_i}}\right)_{Turb} = \frac{1}{(1 + 0.2M^2)^{0.467}} \quad \text{from reference 12} \tag{A2}$$

and

$$\left(\frac{C_f}{C_{f_i}}\right)_{Lam} = \frac{1}{(1 + 0.1305M^2)^{0.12}} \quad \text{from reference 13} \tag{A3}$$

Substituting equations (A2) and (A3) in equation (A1) and solving for x_v, we obtain

$$x_v = \left[\frac{17.932\sqrt{x_{Lam}}\,(1 + 0.2M^2)^{0.467}}{(R/l)^{0.3}\,(1 + 0.1305M^2)^{0.12}}\right]^{1.25} \tag{A4}$$

This length, x_v, was then added to that measured for turbulent flow, x_{Turb} to estimate the total skin friction at each spanwise station. The equivalent turbulent skin friction was then calculated by the more exact logarithmic equation of Schlichting (ref. 14), corrected for compressibility by the more exact temperature-reference method of reference 15. This equation is

$$C_{f_{Equiv\ Turb}} = \frac{0.455(C_f/C_{f_i})_{Turb}}{\left\{\log_{10}[(R/l)(x_{Turb} + x_v)]\right\}^{2.58}} \tag{A5}$$

where

$$\left(\frac{C_f}{C_{f_i}}\right)_{Turb} = \frac{\left(\log_{10}\left\{\left[1 + 0.035M^2 + 0.45\left(\frac{T_w}{T_\infty} - 1\right)\right]^{2.5}\frac{\log_{10}[(R/l)(x_{Turb} + x_v)]}{\log_{10}\left\{\frac{(R/l)(x_{Turb} + x_v)}{T_\infty[1 + 0.035M^2 + 0.45(T_w/T_\infty - 1)] + 198.6}{T_\infty + 198.6}\right\}}\right\}\right)^{2.58}}{1 + 0.035M^2 + 0.45(T_w/T_\infty - 1)} \tag{A6}$$

and

$$T_w/T_\infty = 1 + 0.176M^2$$

for an adiabatic flat plate with an assumed turbulent recovery factor of 0.882. Finally, upon integration of the equivalent turbulent skin-friction coefficients given by equation (A5) across the exposed wing span, we obtain the skin-friction drag coefficient based on a reference area

$$(C_D)_{\text{Lam + Turb}} = \left(\frac{S_{\text{Exp}}}{S}\right)\left\{\left[\int_0^1 C_{f_{\substack{\text{Equiv}\\\text{Turb}}}} \frac{x_{\text{Turb}} + x_v}{(c_{av})_{\text{Exp}}}\, d\left(\frac{y}{b_{\text{Exp}}/2}\right)\right]_{\substack{\text{Upper}\\\text{Surface}}}\right.$$

$$\left. + \left[\int_0^1 C_{f_{\substack{\text{Equiv}\\\text{Turb}}}} \frac{x_{\text{Turb}} + x_v}{(c_{av})_{\text{Exp}}}\, d\left(\frac{y}{b_{\text{Exp}}/2}\right)\right]_{\substack{\text{Lower}\\\text{Surface}}}\right\} \qquad \text{(A7)}$$

where

$(c_{av})_{\text{Exp}}$ average chord of exposed area

$d\left(\frac{y}{b_{\text{Exp}}/2}\right)$ dimensionless spanwise differential element

A similar analysis also was performed on the body to calculate its contribution to the skin-friction drag. No additional corrections were applied for three-dimensional effects on the body-nose and the wing-body juncture. In the computations for the all-turbulent boundary layer, equation (A7) was used with $x_v = 0$ and $x_{\text{Turb}} = c$. The increment of drag coefficient added to each measured drag coefficient (transition free) to adjust the drag data to conditions corresponding to an all-turbulent boundary layer is

$$\Delta C_D = (C_{D_{Sf}})_{\text{Turb}} - (C_{D_{Sf}})_{\text{Lam + Turb}}$$

APPENDIX B

DRAG DUE TO LEADING-EDGE THICKNESS

The method developed herein is applicable only to a supersonic leading edge. With the leading edge subsonic, no correction for leading-edge thickness was made; however, theory predicts a leading-edge thrust force which does not usually occur in a real fluid.

For a cylindrical leading edge (see sketch) with zero sweep ($\Lambda = 0$) the

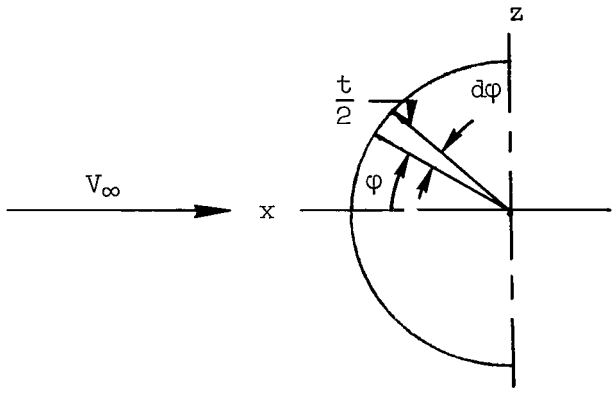

pressure coefficient is

$$C_p = C_{p_{max}} \cos^2 \varphi \tag{B1}$$

where

φ angle measured from the stagnation point ($z = 0$), radians

$C_{p_{max}}$ pressure coefficient at the stagnation point

The drag coefficient for a differential length of leading edge based on the leading-edge thickness t is

$$C_{D_l} = \frac{D_l}{t q_\infty} = \frac{1}{t} \int_{-\frac{\pi}{2}}^{\frac{\pi}{2}} C_p \, dz \tag{B2}$$

where

$$dz = \frac{t}{2} \cos \varphi \, d\varphi$$

hence,

$$C_{D_l} = \frac{1}{2} \int_{-\frac{\pi}{2}}^{\frac{\pi}{2}} C_{p_{max}} \cos^3 \varphi \, d\varphi$$

$$= \frac{2}{3} C_{p_{max}} \tag{B3}$$

To find the drag coefficient for the entire leading edge based on the wing area S multiply C_{D_l} by (tL/S); that is

$$C_{D_{\Lambda=0}} = \frac{2}{3} C_{p_{max}} \left(\frac{tL}{S}\right) \tag{B4}$$

where L is the length of the leading edge with constant thickness, t. Now $C_{p_{max}}$ is the pressure coefficient behind a detached shock wave at the leading edge; that is,

$$C_{p_{max}} = \frac{P_{t_2} - P_\infty}{q_\infty} \tag{B5}$$

where P_{t_2} is the stagnation pressure at the leading edge and P_∞ is the free-stream static pressure. If it is assumed that the small portion of the detached shock wave directly in front of the leading edge is normal, $C_{p_{max}}$ can be found from supersonic flow tables (ref. 16) as

$$C_{p_{max}} = \left(\frac{P_{t_2}}{P_{t_1}}\right)\left(\frac{P_{t_1}}{q_\infty}\right) - \left(\frac{P_\infty}{P_{t_1}}\right)\left(\frac{P_{t_1}}{q_\infty}\right) \tag{B6}$$

where

P_{t_1} total pressure ahead of the normal shock wave

P_{t_2} total pressure behind the normal shock wave

P_∞ free-stream static pressure

q_∞ free-stream dynamic pressure

If the leading edge makes an angle of Λ with the direction of flow, the dynamic pressure forces acting on the leading edge correspond to the velocity component normal to the edge; hence,

$$C_{D_{normal}} = C_{D_{\Lambda=0}} \cos^2 \Lambda \tag{B7}$$

Now the drag coefficient due to bluntness on a swept leading edge is the component of $C_{D_{normal}}$ parallel to the direction of flow. Therefore,

$$C_{D_\Lambda} = C_{D_{\Lambda=o}} \cos^3 \Lambda$$

$$= \frac{2}{3} C_{p_{max}} \left(\frac{tL}{S}\right) \cos^3 \Lambda \tag{B8}$$

or for wings with straight leading edges, $L \cos \Lambda = b_{Exp}$ and

$$C_{D_\Lambda} = \frac{2}{3} C_{p_{max}} \frac{tb_{Exp}}{S} \cos^2 \Lambda \tag{B9}$$

For wings with curved leading edges, equation (B8) must be integrated along the span from the wing root to the wing tip;

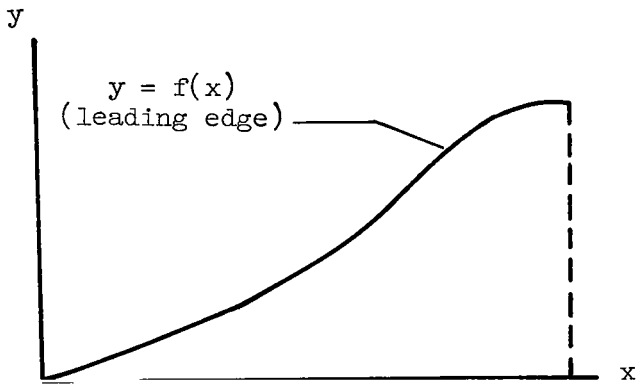

that is,

$$C_{D_\Lambda} = \frac{2}{3} C_{p_{max}} \left(\frac{t}{S}\right) \int_o^{b_{Exp}} \cos^3 \Lambda_l \, dL \tag{B10}$$

where the local leading-edge sweep angle

$$\Lambda_l = \cot^{-1} \frac{dy}{dx}$$

and

$$dL = dy \sqrt{1 + \left(\frac{dx}{dy}\right)^2}$$

REFERENCES

1. Jones, Robert T.: Estimated Lift-Drag Ratios at Supersonic Speeds. NACA TN 1350, 1947.

2. Beane, B. J.: Curves of Minimum Wave Plus Vortex Drag Coefficient for Several Wing Plan Forms. Rep. SM-22989, Douglas Aircraft Co., Nov. 1957.

3. Hopkins, Edward J., Jillie, Don W., and Levin, Alan D.: Lift, Drag, and Pitching Moments of an Arrow Wing Having 80° of Sweepback at Mach Numbers From 2.48 to 3.51 and Reynolds Numbers up to 11.0 Million. NASA TM X-22, 1959.

4. Hopkins, Edward J.: Lift, Pitching Moment and Span Load Distribution of Wings at Low Speed as Affected by Variations of Sweep and Aspect Ratio. NACA TN 2284, 1951.

5. Pitts, William C., Nielsen, Jack N., and Kaattari, George E.: Lift and Center of Pressure of Wing-Body-Tail Combinations at Subsonic, Transonic, and Supersonic Speeds. NACA Rep. 1307, 1957.

6. Lomax, Harvard, and Sluder, Loma: Chordwise and Compressibility Corrections to Slender-Wing Theory. NACA Rep. 1105, 1952.

7. DeYoung, John, and Harper, Charles W.: Theoretical Symmetric Span Loading at Subsonic Speeds for Wings Having Arbitrary Plan Form. NACA Rep. 921, 1948.

8. Eichelbrenner, E. A.: Lift of Arrow Wings. Recherche Aêronaut 25, 1952, p. 19-20.

9. Lapin, Ellis: Charts for the Computation of Lift and Drag of Finite Wings at Supersonic Speeds. Rep. SM-13480, Douglas Aircraft Co., 1949.

10. Jones, R. T.: Theory of Wing-Body Drag at Supersonic Speeds. NACA Rep. 1284, 1956.

11. Locke, F. W. S., Jr.: Recommended Definition of Turbulent Friction in Incompressible Fluids. BuAer, Navy Dept., (Design) Res. Div., DR Rep. 1415, 1952.

12. Rubesin, Morris W., Maydew, Randall C., and Varga, Steven A.: An Analytical and Experimental Investigation of the Skin Friction of the Turbulent Boundary Layer on a Flat Plate at Supersonic Speeds. NACA TN 2305, 1951.

13. Johnson, H. A., and Rubesin, M. W.: Aerodynamic Heating and Convective Heat Transfer - Summary of Literature Survey. Trans. ASME, 71, 1949, pp. 447-456.

14. Schlichting, Hermann: Boundary Layer Theory (Trans. by J. Kestin). New York, McGraw, 1955, p. 540.

15. Sommer, Simon C., and Short, Barbara J.: Free-Flight Measurements of Turbulent Boundary-Layer Skin Friction in the Presence of Severe Aerodynamic Heating at Mach Numbers From 2.8 to 7.0. NACA TN 3391, 1955.

16. Ames Research Staff: Equations, Tables, and Charts for Compressible Flow. NACA Rep. 1135, 1953. (Supersedes NACA TN 1428)

TABLE I.- SKIN-FRICTION AND BLUNTNESS-DRAG CORRECTIONS

Triangular wing			Trapezoidal wing		
M	$(C_{D_{Sf}})_{Turb} - (C_{D_{Sf}})_{Lam + Turb}$	$(C_D)_{due\ to\ leading\ edge\ bluntness}$	M	$(C_{D_{Sf}})_{Turb} - (C_{D_{Sf}})_{Lam + Turb}$	$(C_D)_{due\ to\ leading\ edge\ bluntness}$
0.7	0.0032	0	0.7	0.0036	0
.9	.0033	0	.9	.0040	0
1.0	.0034	0	1.0	.0044	0
1.1	.0036	0	1.1	.0051	.0021
1.4	.0039	0	1.4	.0058	.0024
1.98	.0027	.0007	1.98	.0038	.0027
2.94	.0027	.0007	2.94	.0033	.0028
Modified trapezoidal wing			Ogee wing		
.7	.0030	0	.7	.0025	0
.9	.0032	0	.9	.0028	0
1.0	.0033	0	1.0	.0028	0
1.1	.0037	0	1.1	.0031	0
1.4	.0042	.0010	1.4	.0037	.0003
1.98	.0034	.0012	1.98	.0028	.0006
2.94	.0030	.0012	2.94	.0024	.0007

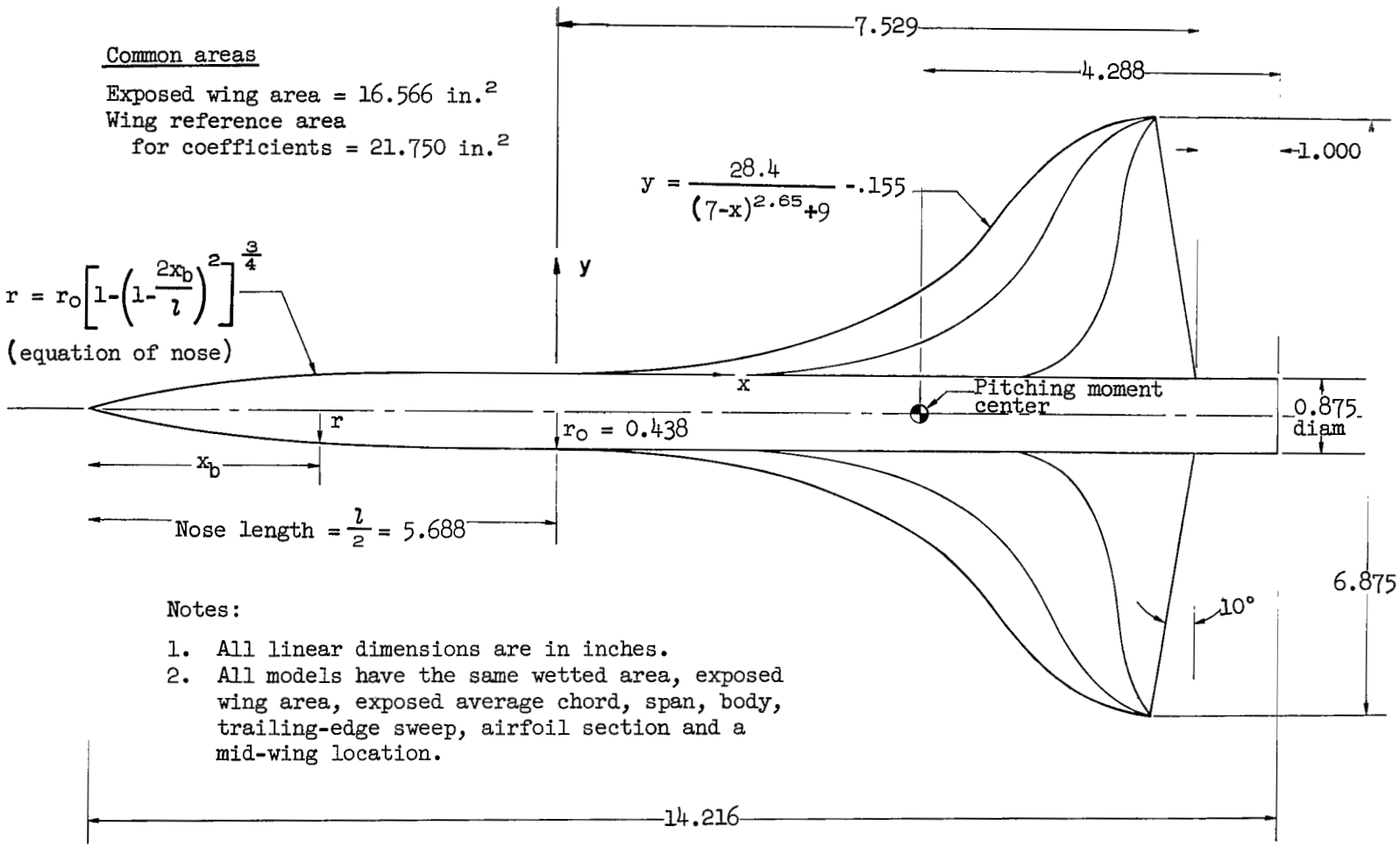

(a) Ogee wing.

Figure 1.- Model dimensions.

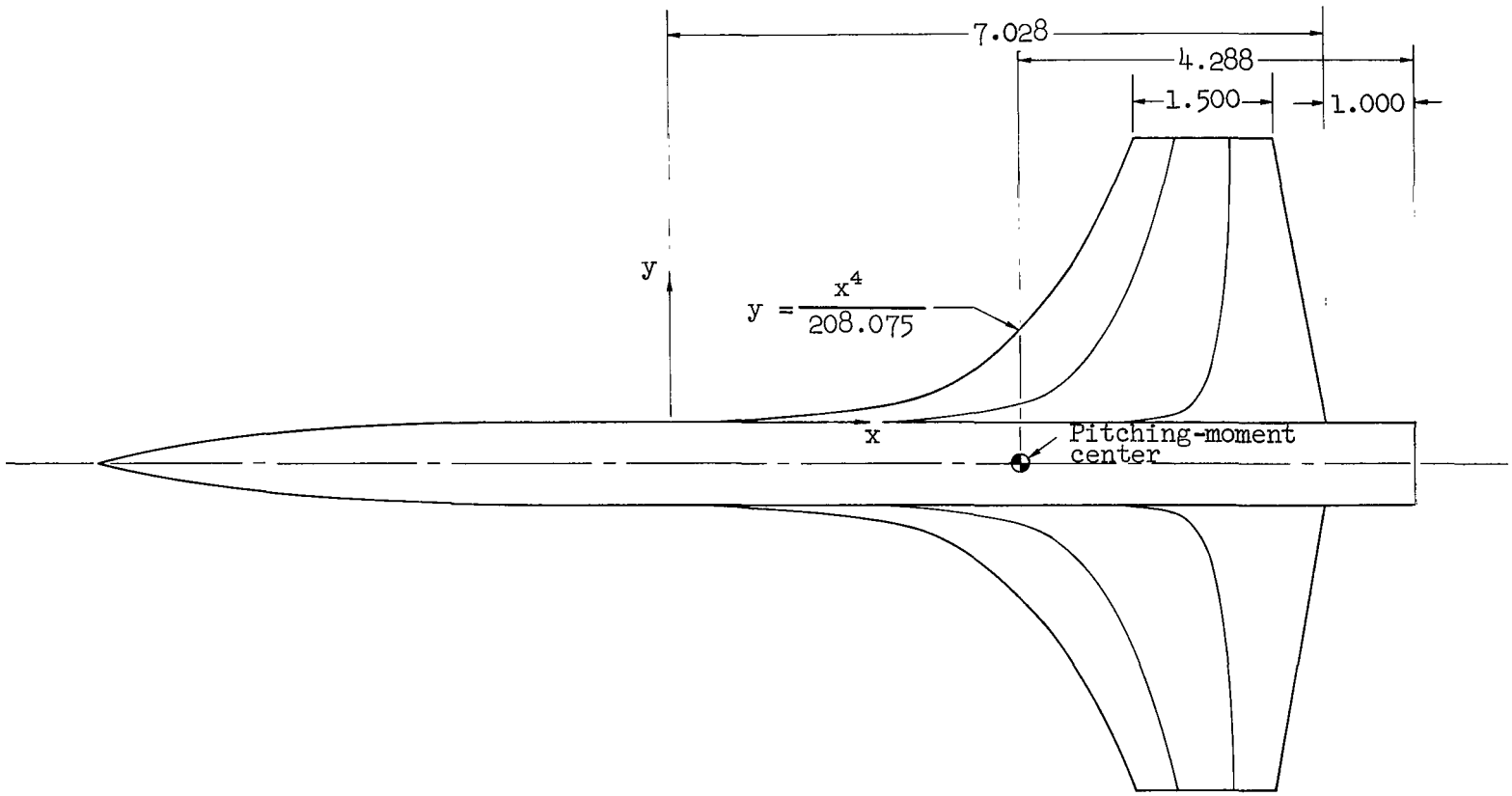

(b) Modified trapezoidal wing.

Figure 1.- Continued.

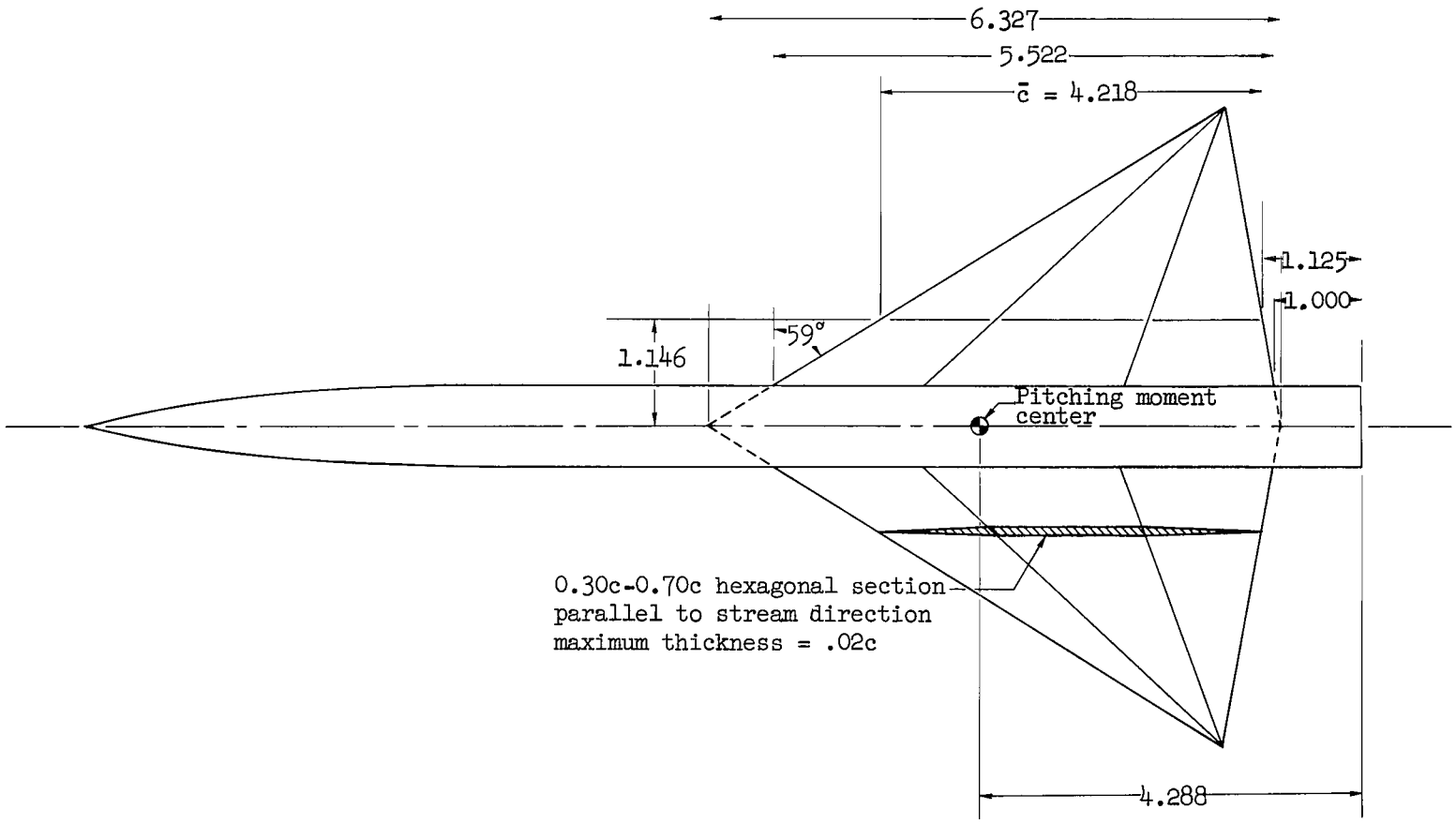

(c) Triangular wing.

Figure 1.- Continued.

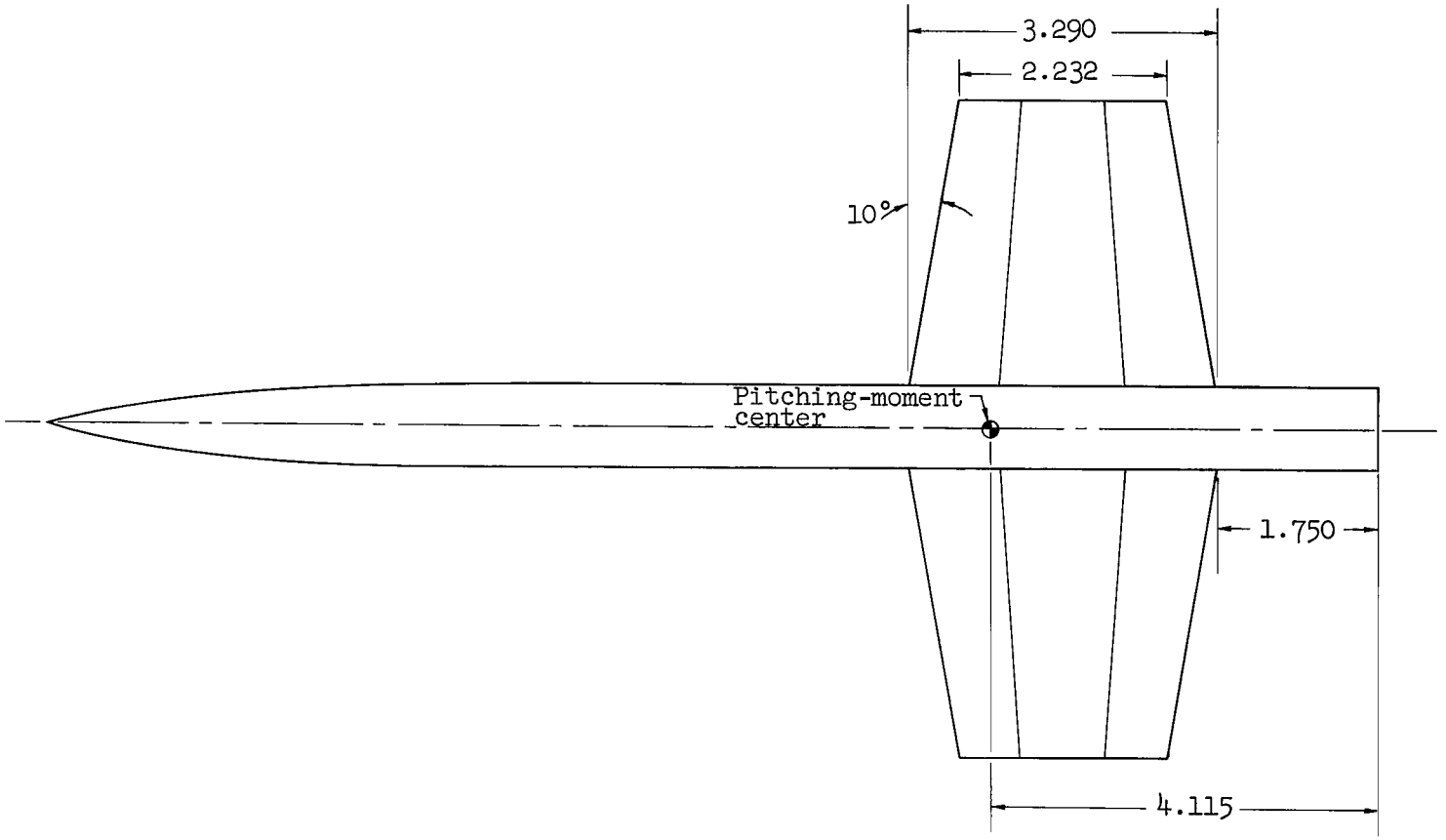

(d) Trapezoidal wing.

Figure 1.- Concluded.

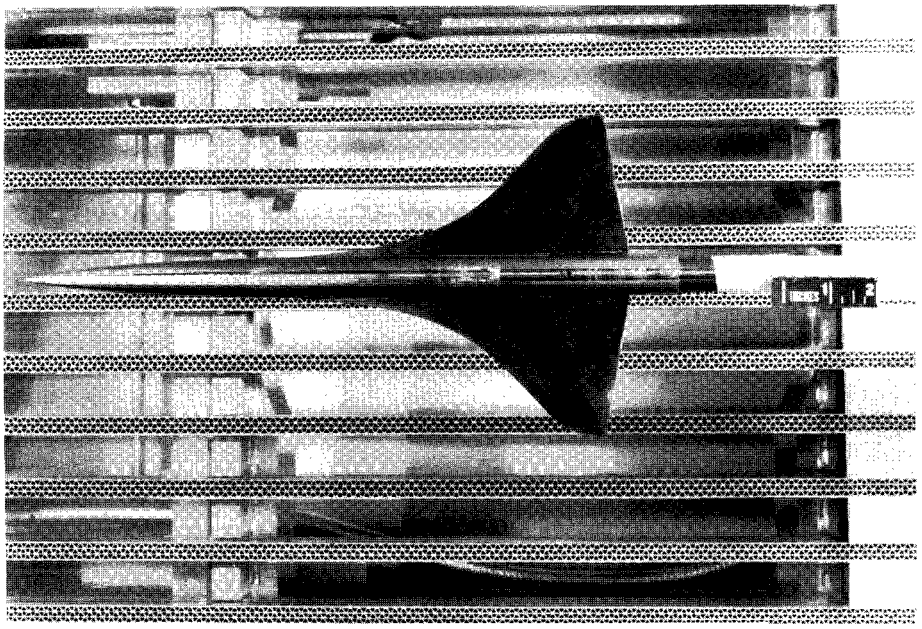

A-31516

(a) Ogee wing.

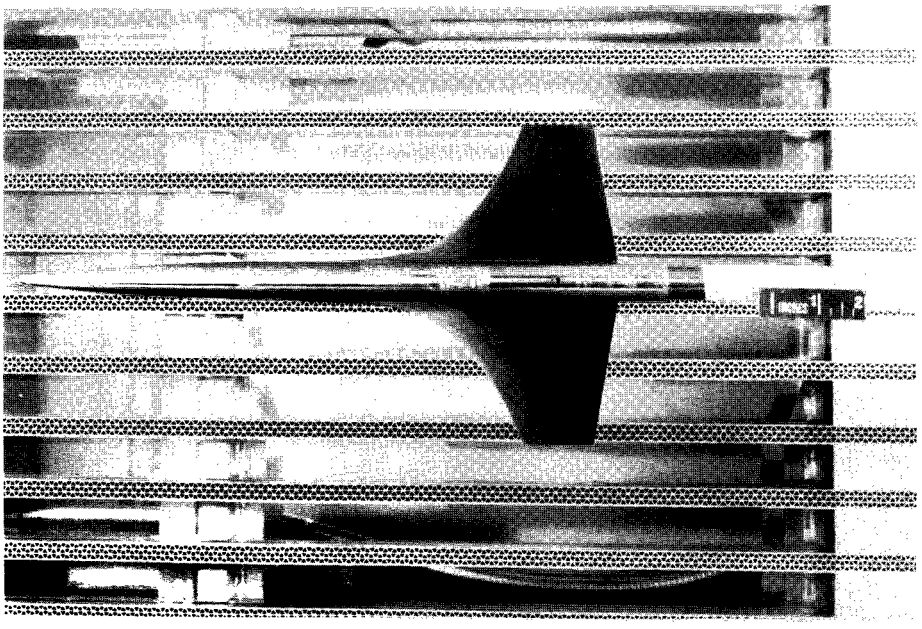

A-31513

(b) Modified trapezoidal wing.

Figure 2.- Wing-body combinations in the Ames 2- by 2-foot wind tunnel.

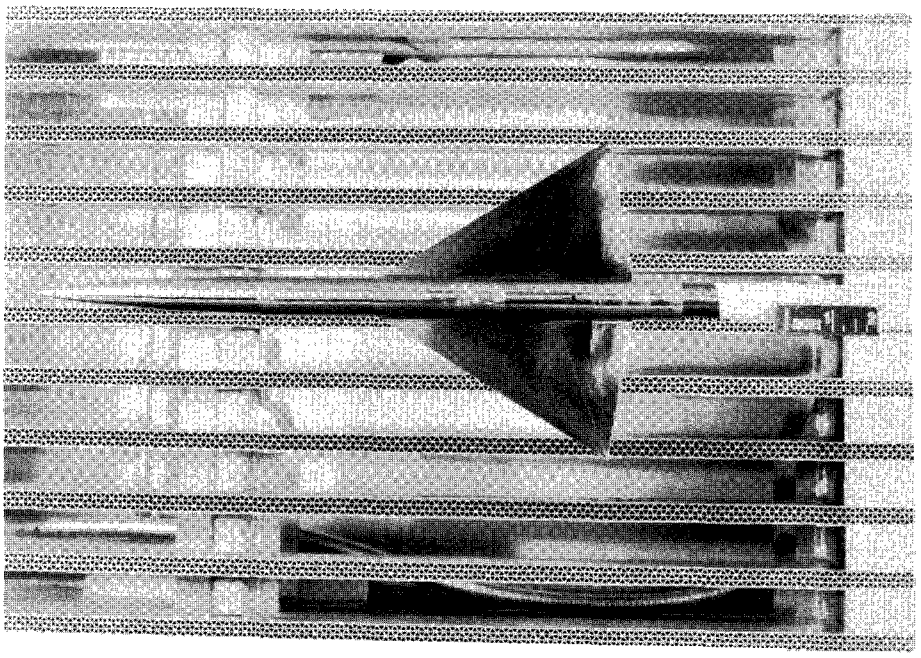

A-31515

(c) Triangular wing.

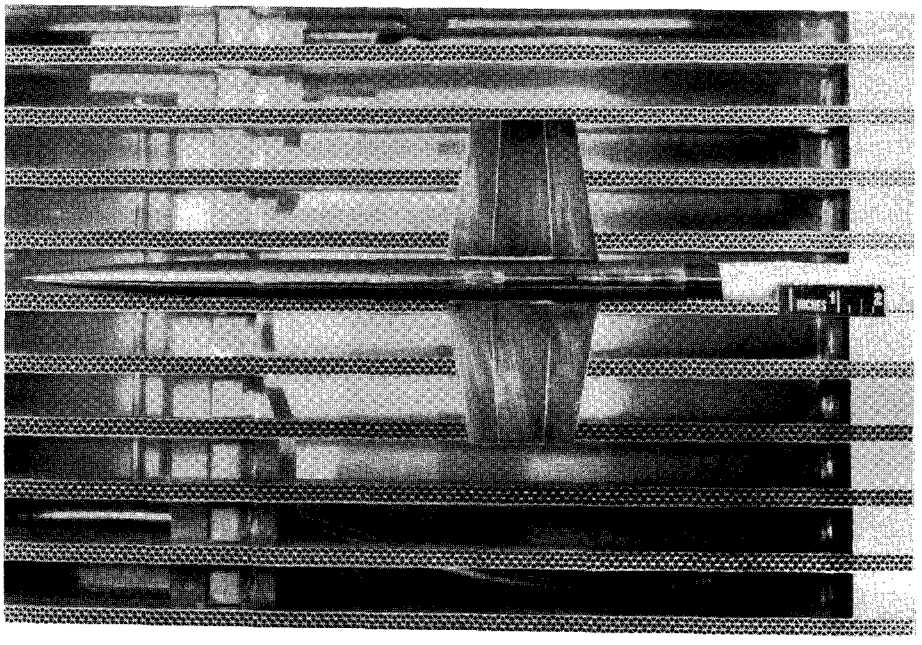

A-31514

(d) Trapezoidal wing.

Figure 2.- Concluded.

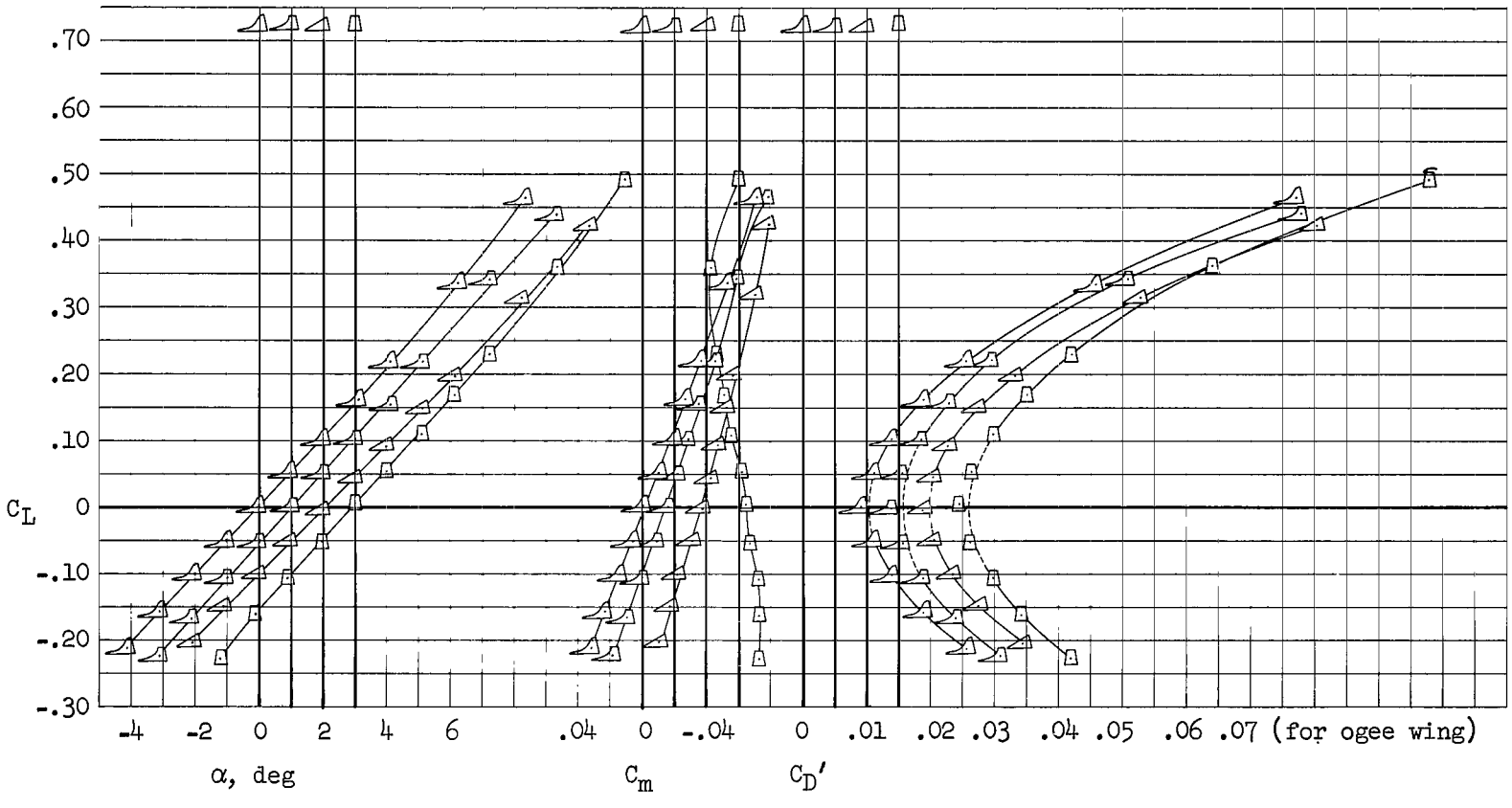

(a) C_L vs α, C_m and C_D'

Figure 3.- Comparison of lift, drag, pitching moment, and drag due to lift for the ogee, modified trapezoidal, triangular, and trapezoidal wings; M = 0.70.

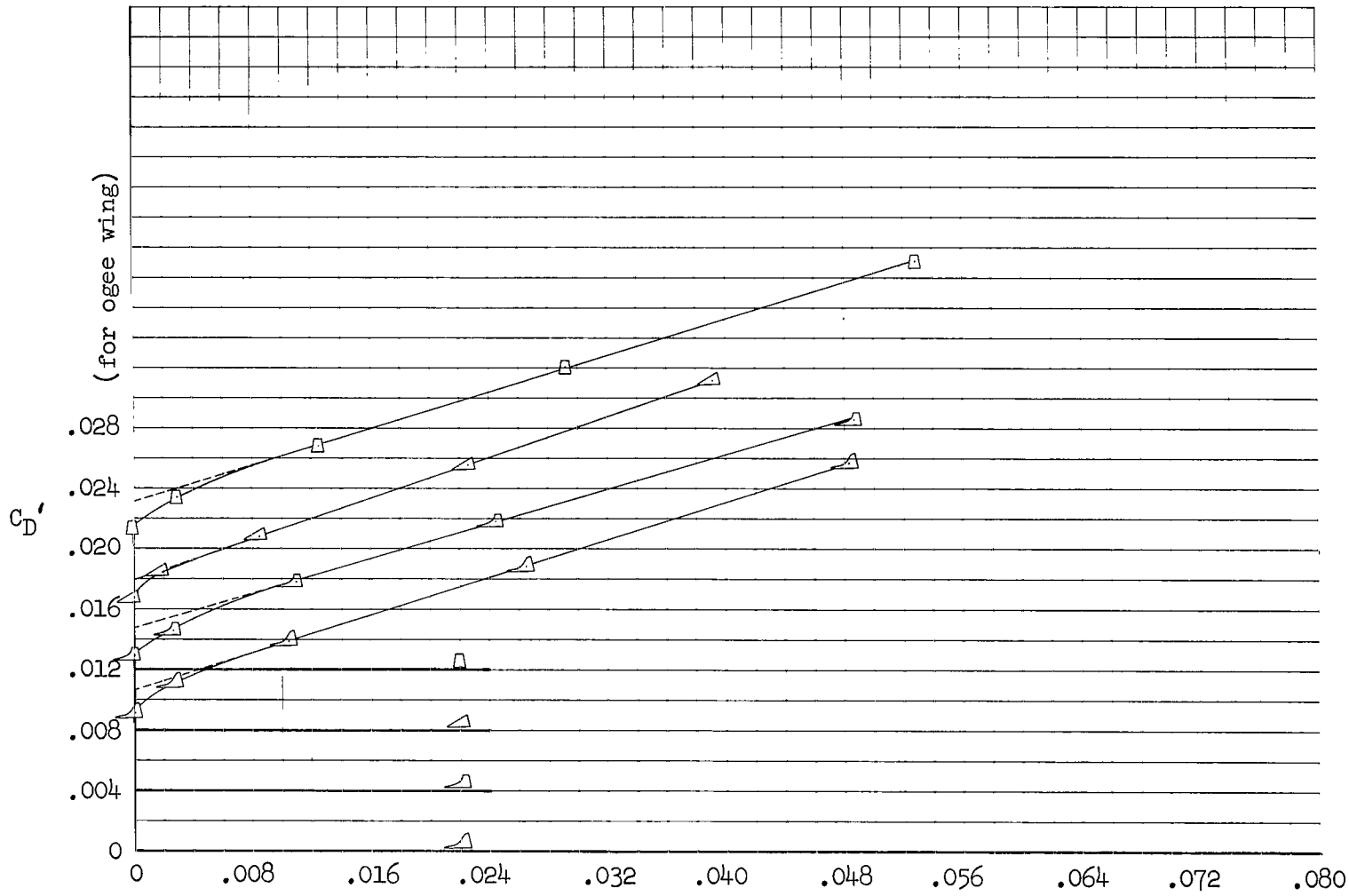

(b) C_D' vs C_L^2

Figure 3.- Concluded.

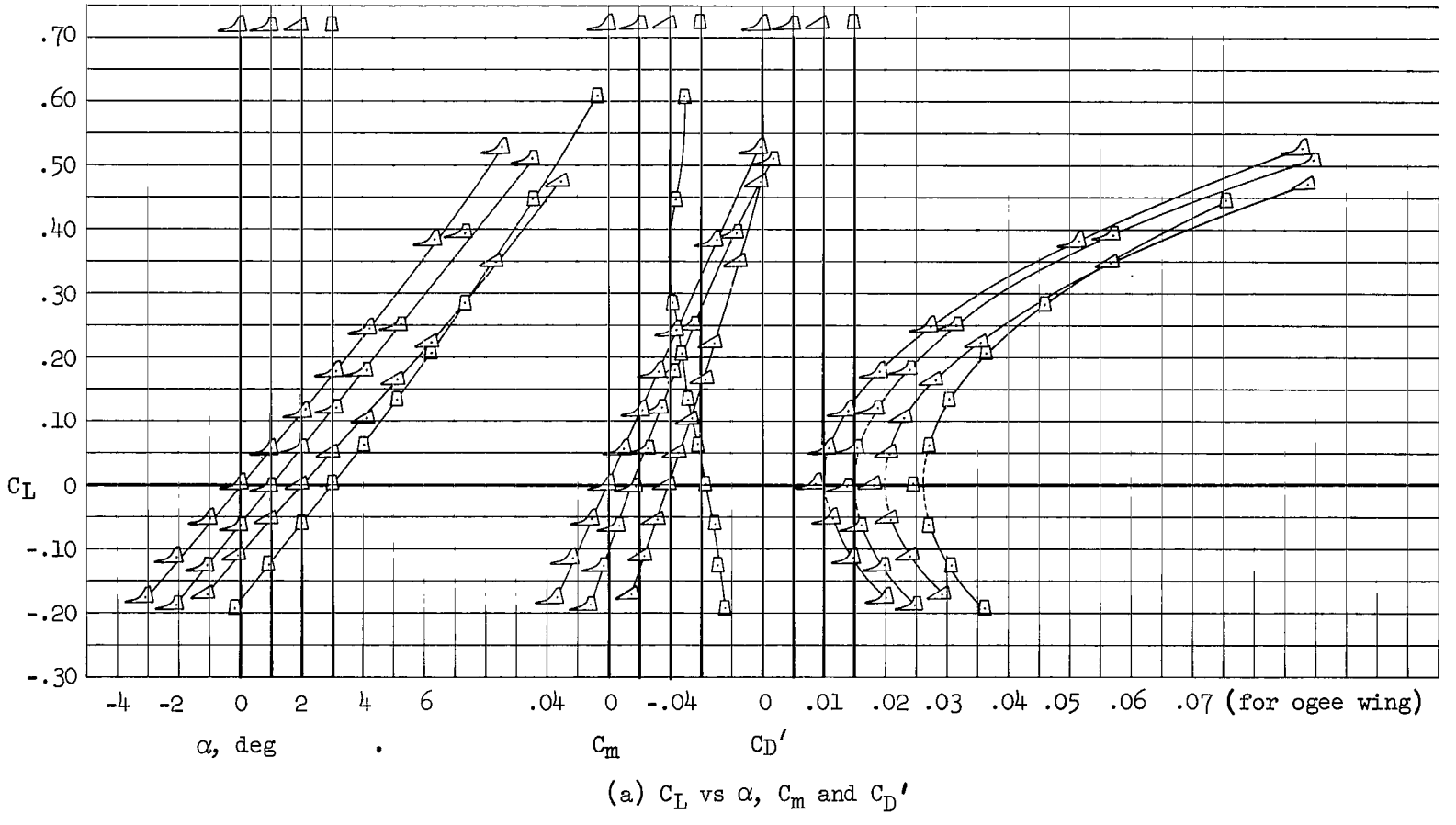

(a) C_L vs α, C_m and C_D'

Figure 4.- Comparison of lift, drag, pitching moment, and drag due to lift for the ogee, modified trapezoidal, triangular, and trapezoidal wings; M = 0.90.

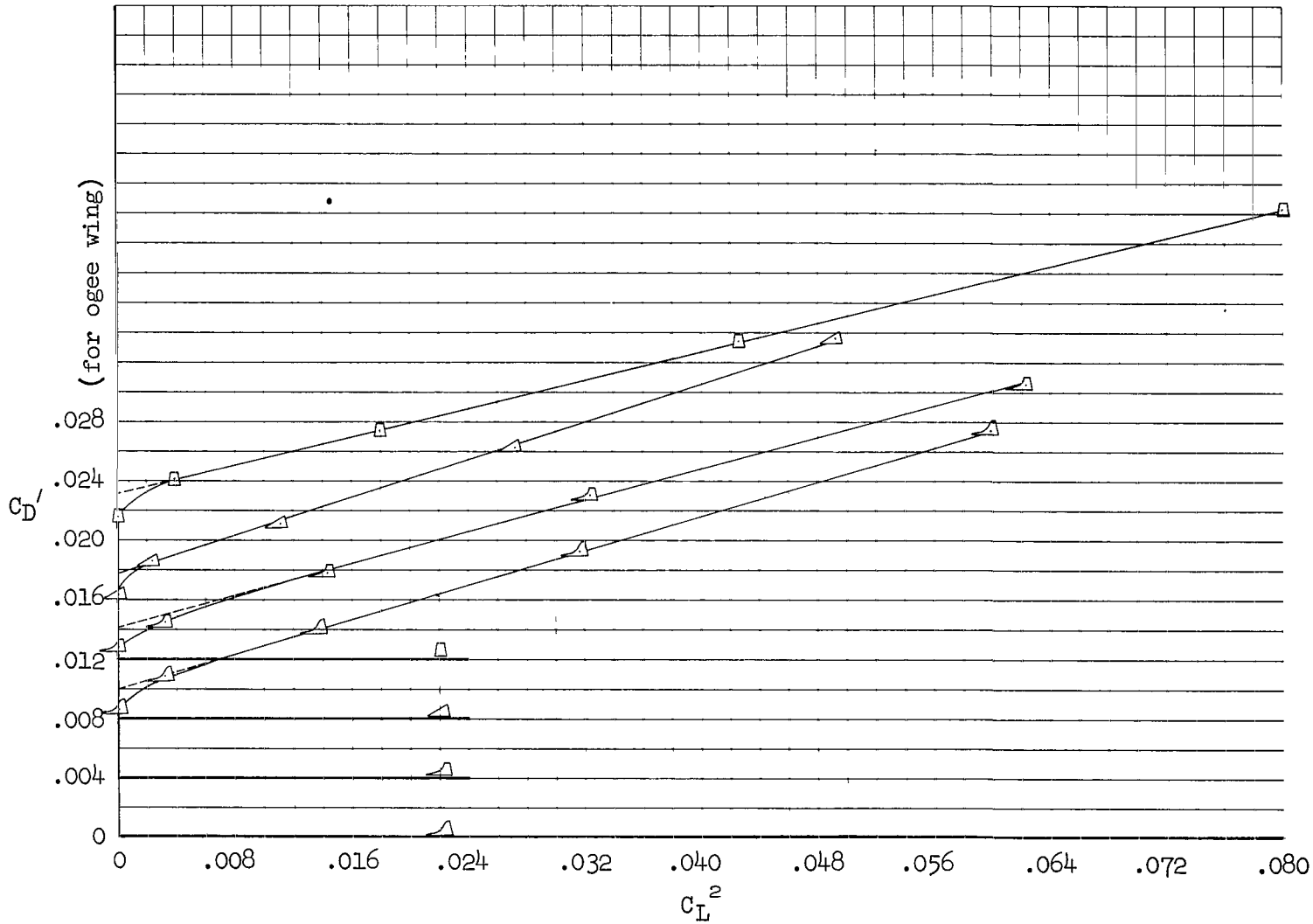

(b) C_D' vs C_L^2

Figure 4.- Concluded.

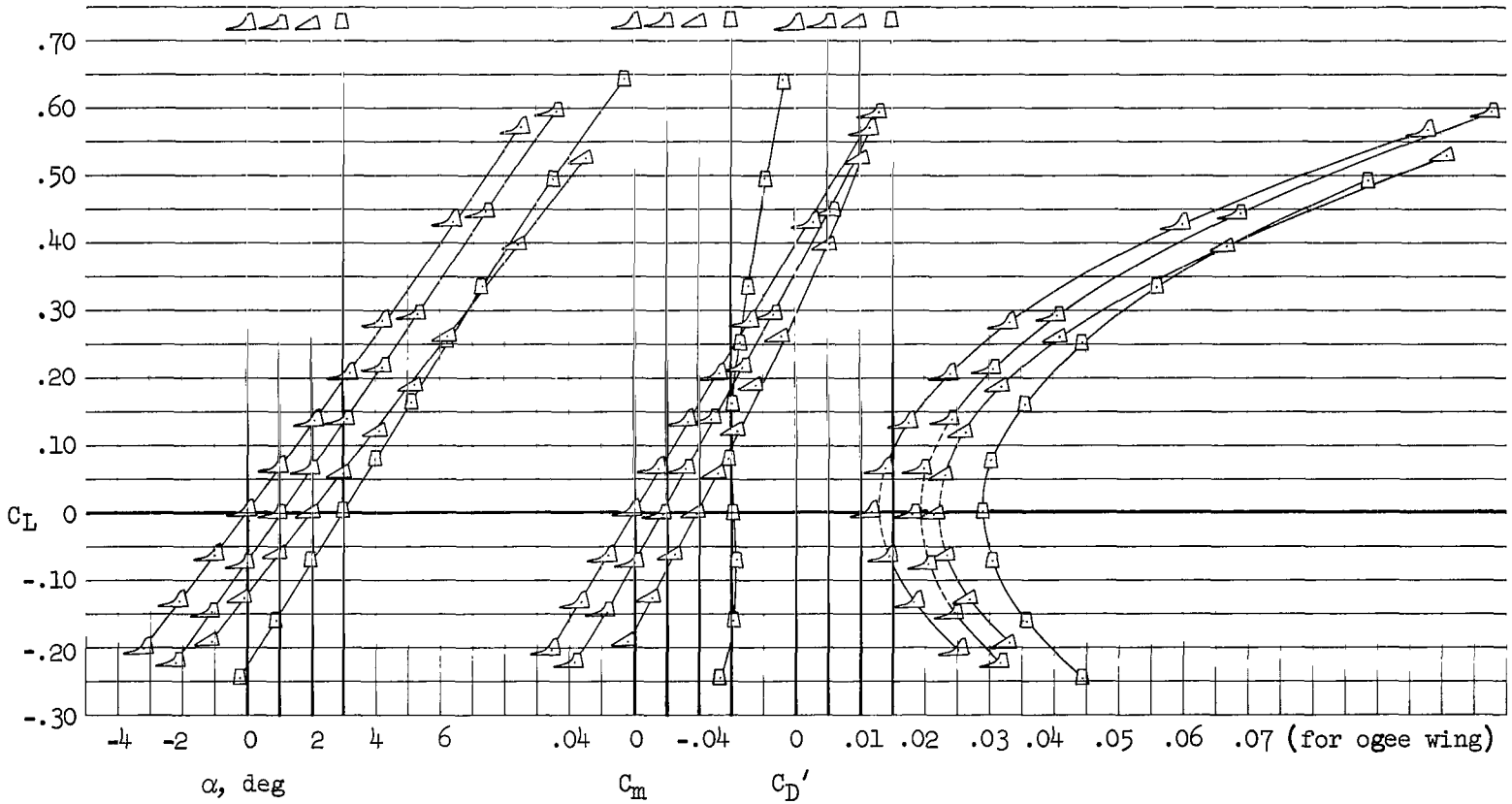

(a) C_L vs α, C_m and C_D'

Figure 5.- Comparison of lift, drag, pitching moment, and drag due to lift for the ogee, modified trapezoidal, triangular, and trapezoidal wings; M = 1.00.

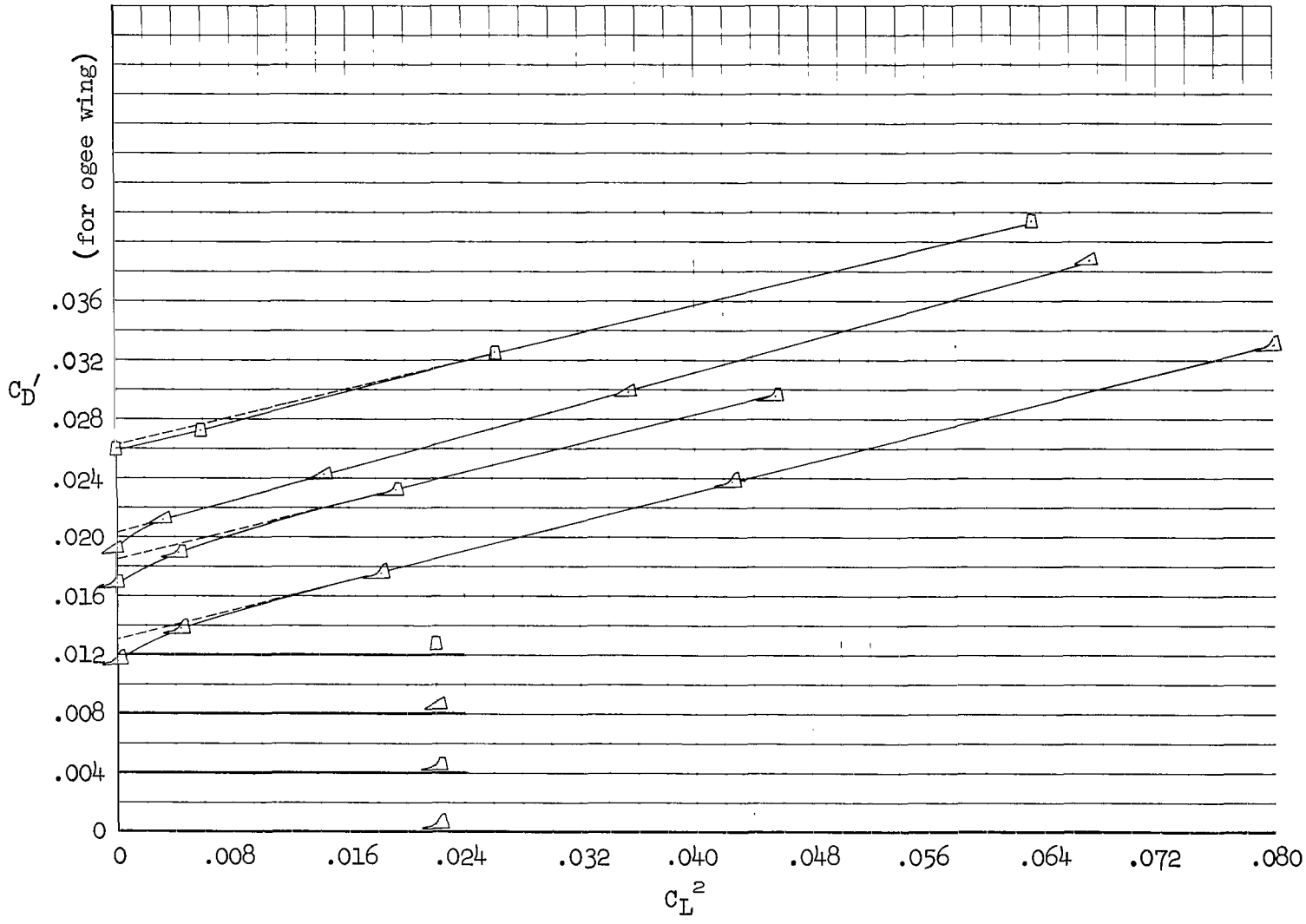

(b) C_D' vs C_L^2

Figure 5.- Concluded.

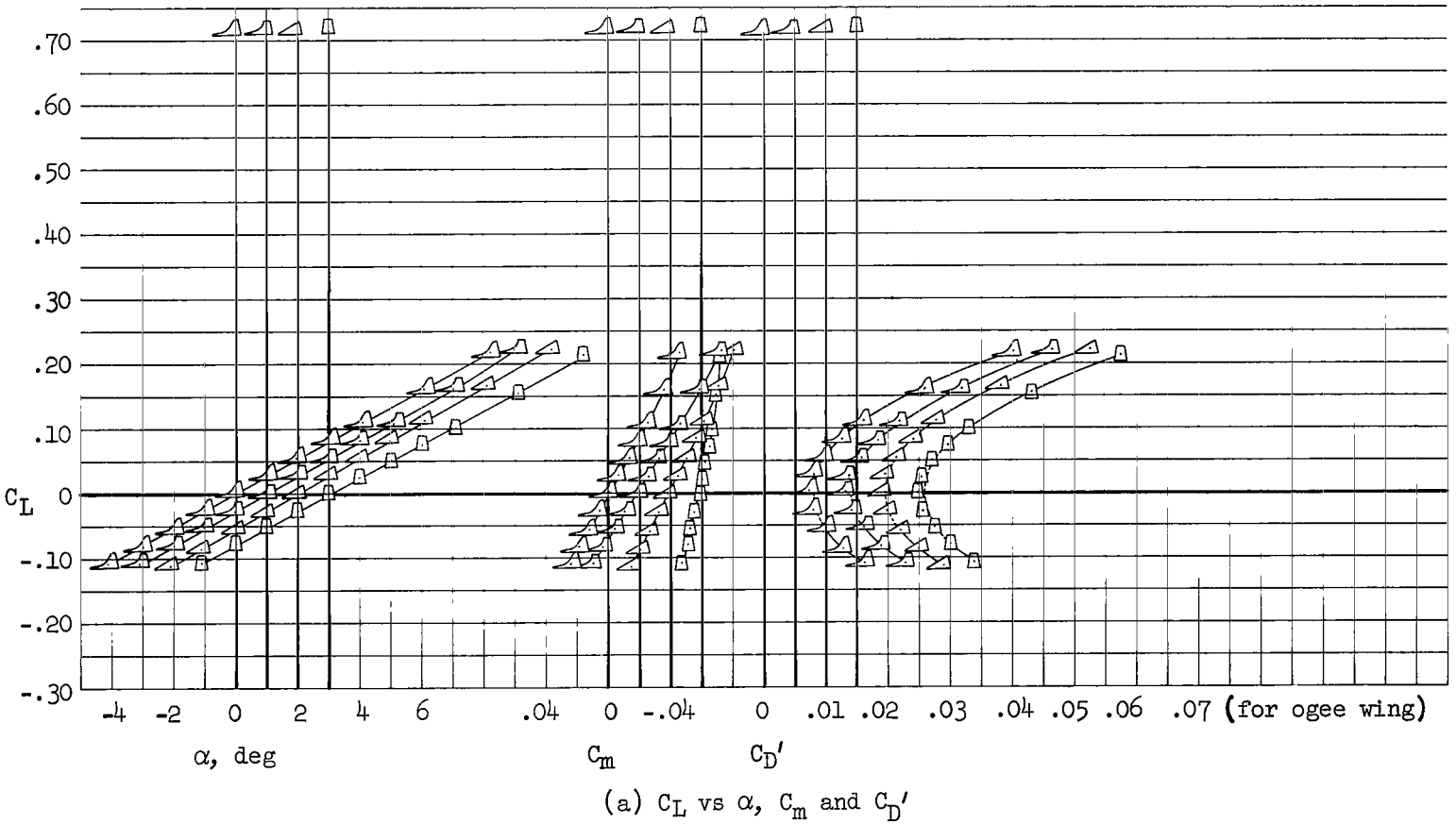

(a) C_L vs α, C_m and C_D'

Figure 9.- Comparison of lift, drag, pitching moment, and drag due to lift for the ogee, modified trapezoidal, triangular, and trapezoidal wings; M = 2.94.

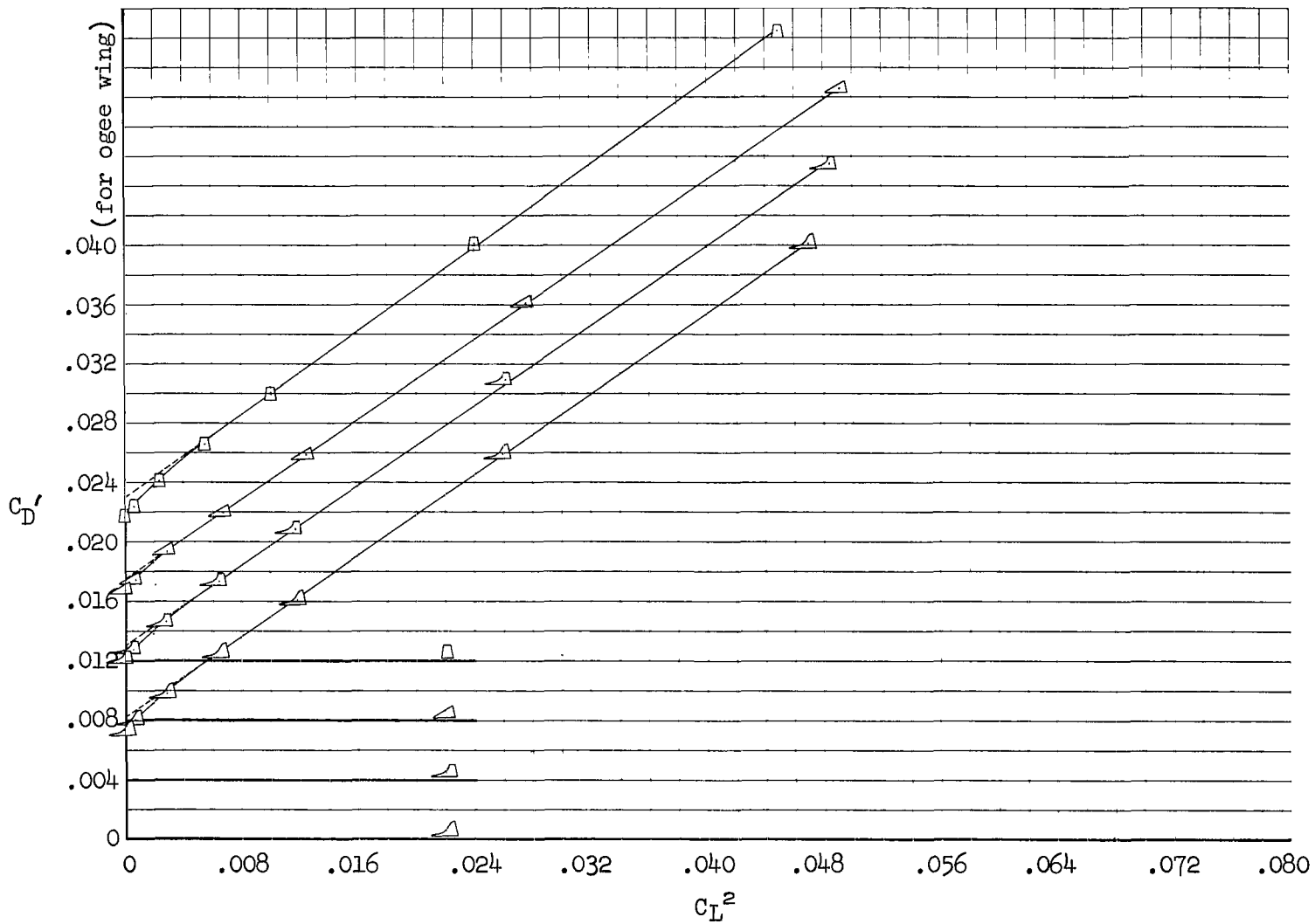

(b) C_D' vs C_L^2

Figure 9.- Concluded.

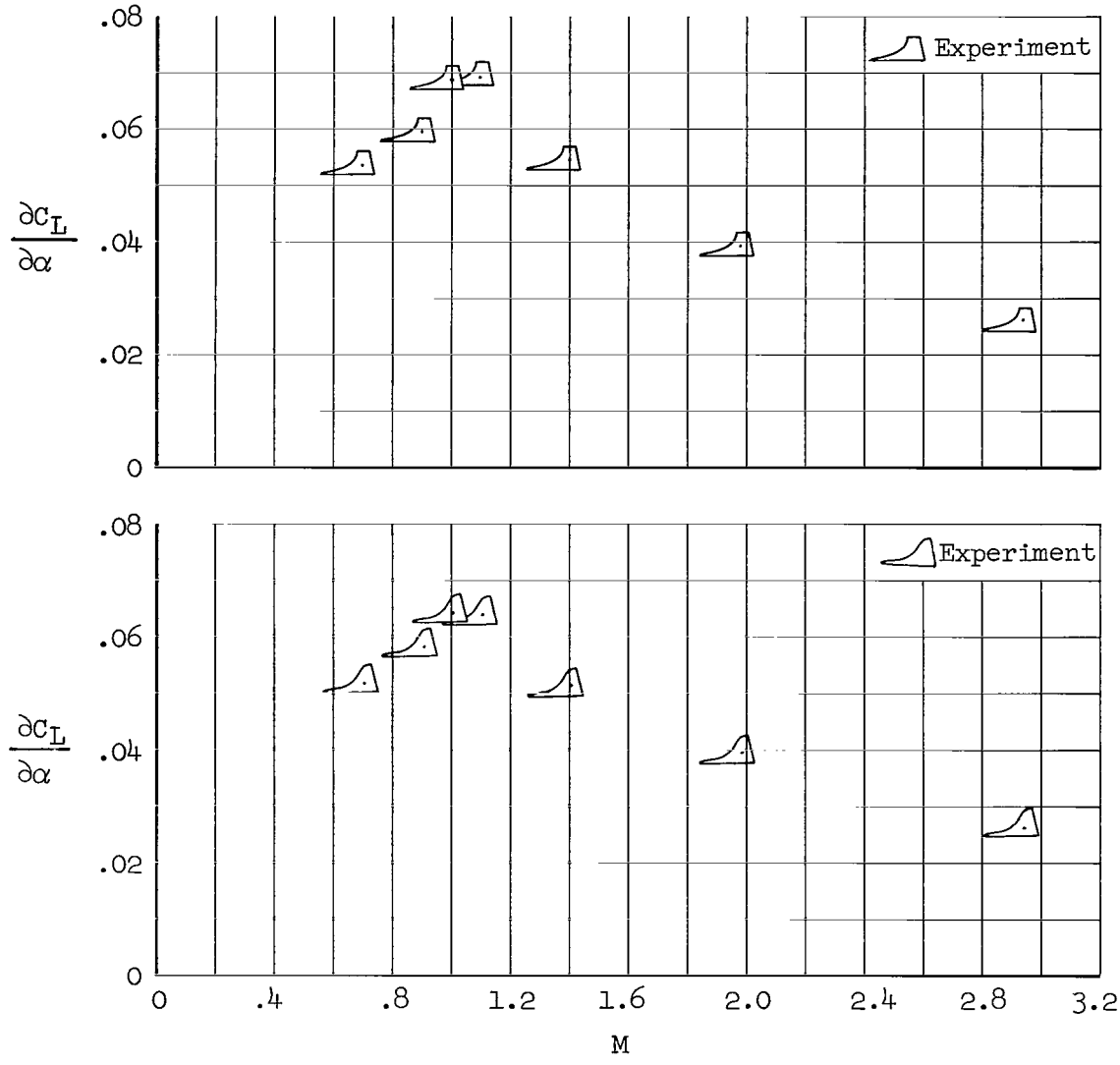

(a) Modified trapezoidal and ogee wings.

Figure 10.- Lift-curve slope as a function of Mach number.

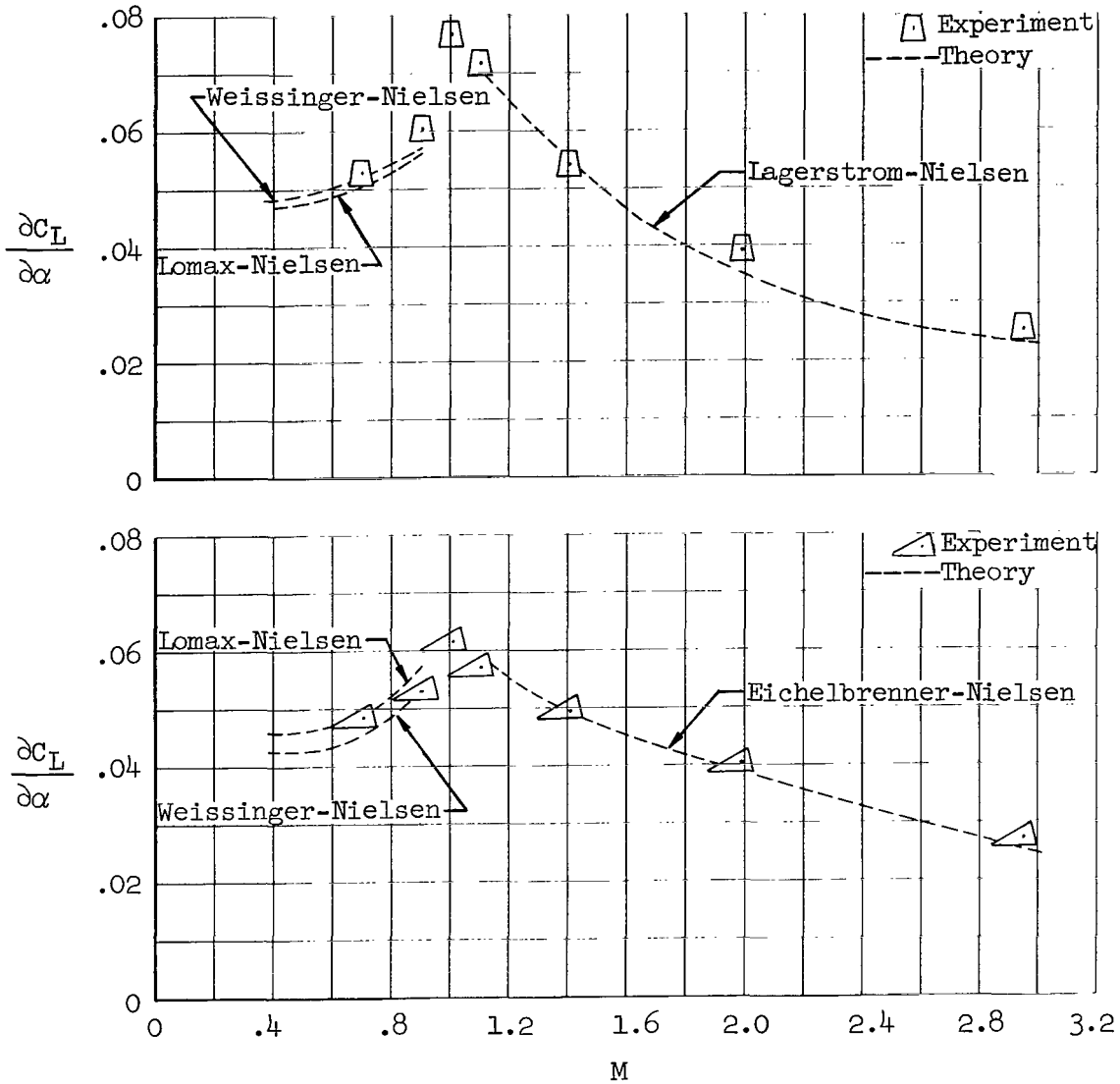

(b) Trapezoidal and triangular wings.

Figure 10.- Concluded.

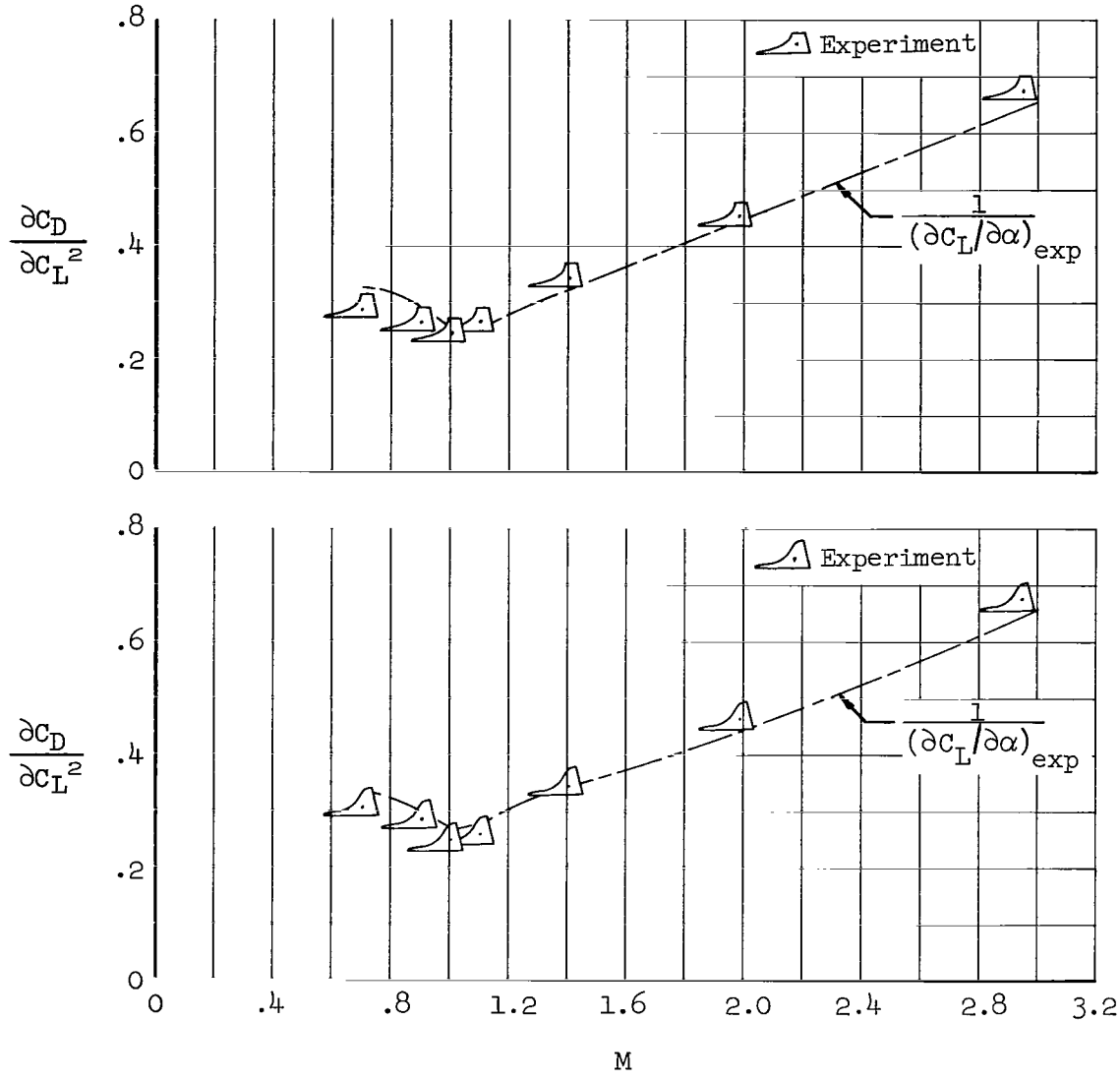

(a) Modified trapezoidal and ogee wings.

Figure 11.- Drag-rise factor as a function of Mach number.

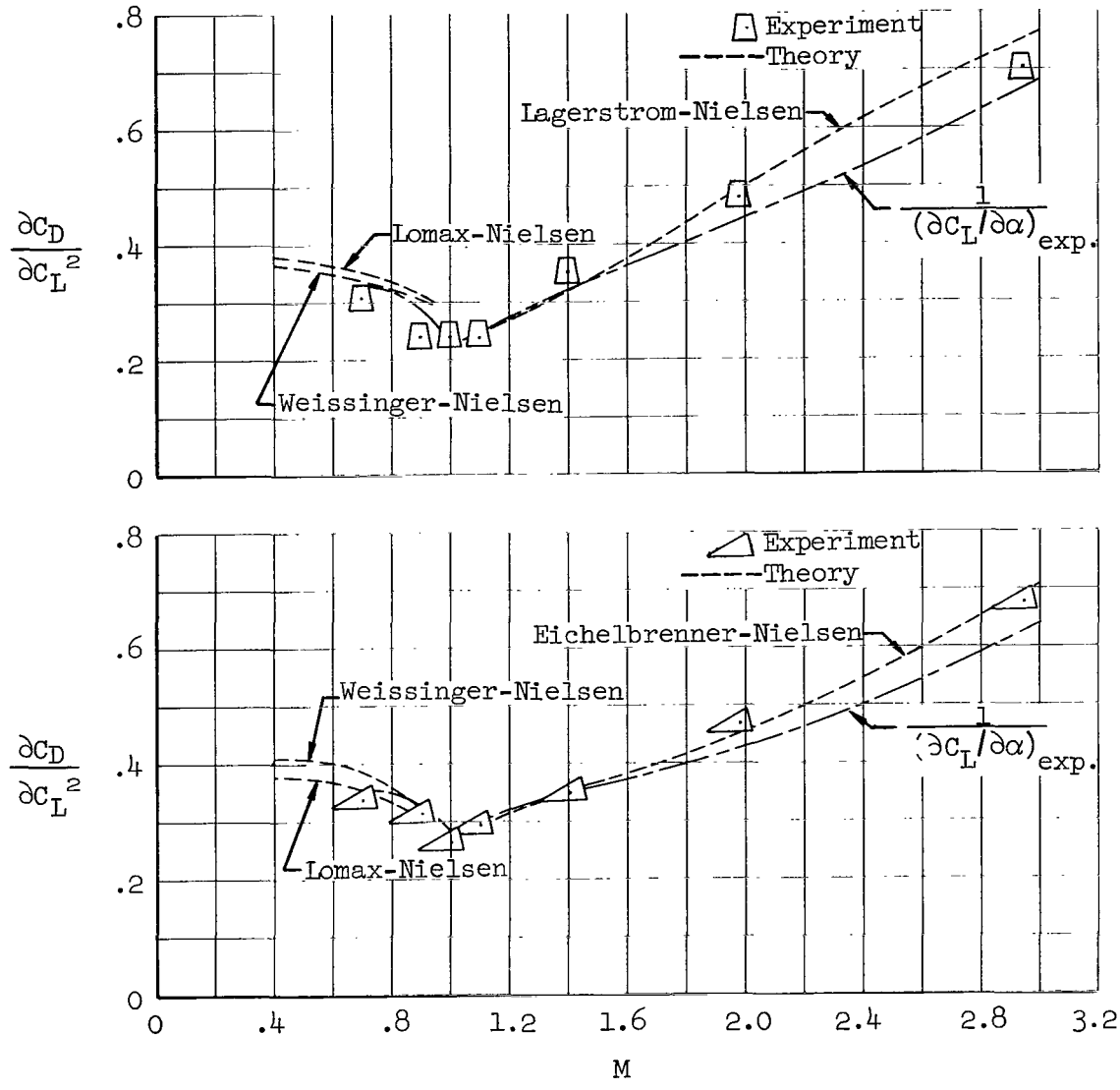

(b) Trapezoidal and triangular wings.

Figure 11.- Concluded.

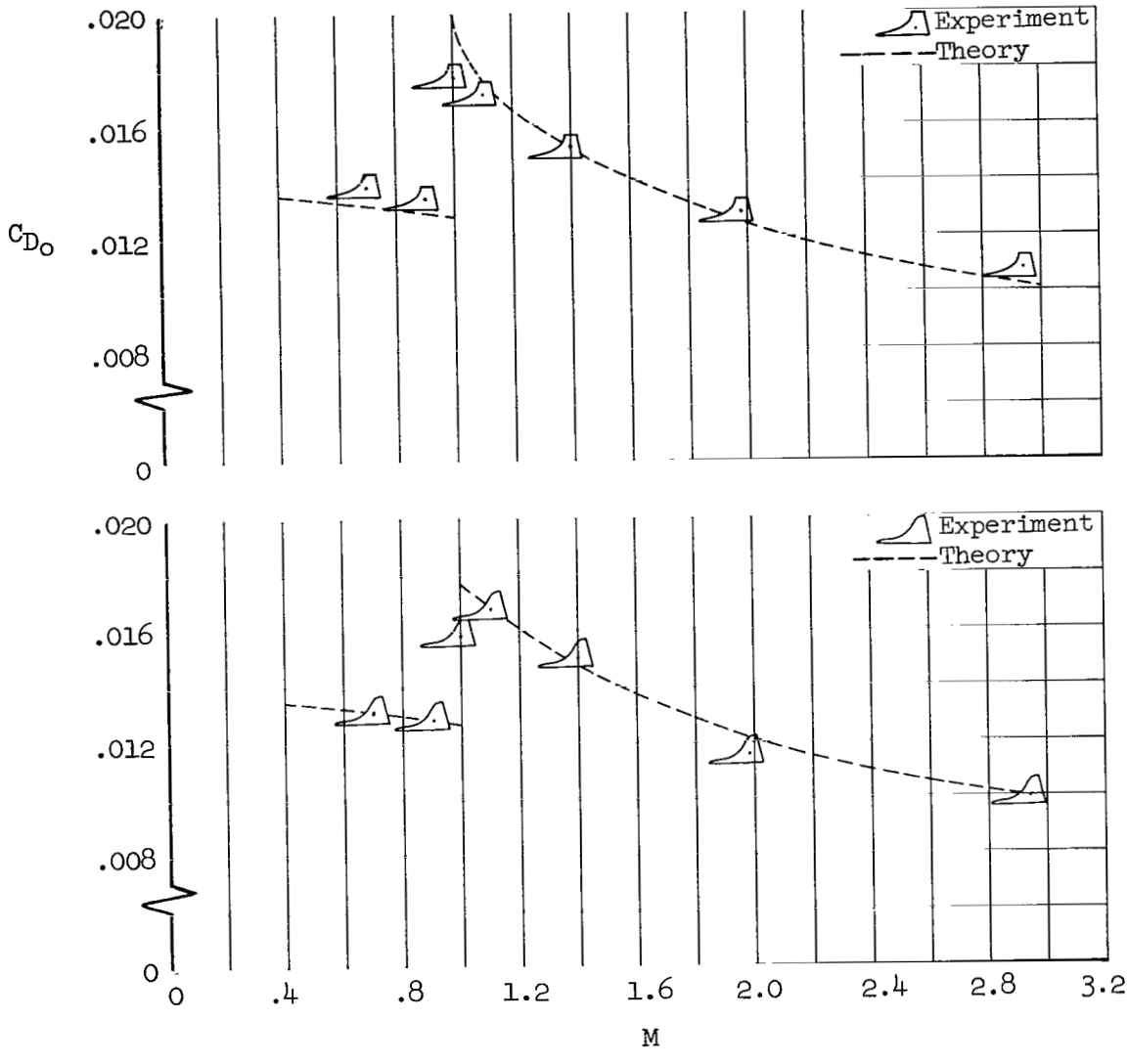

(a) Modified trapezoidal and ogee wings.

Figure 12.- Minimum drag coefficient as a function of Mach number.

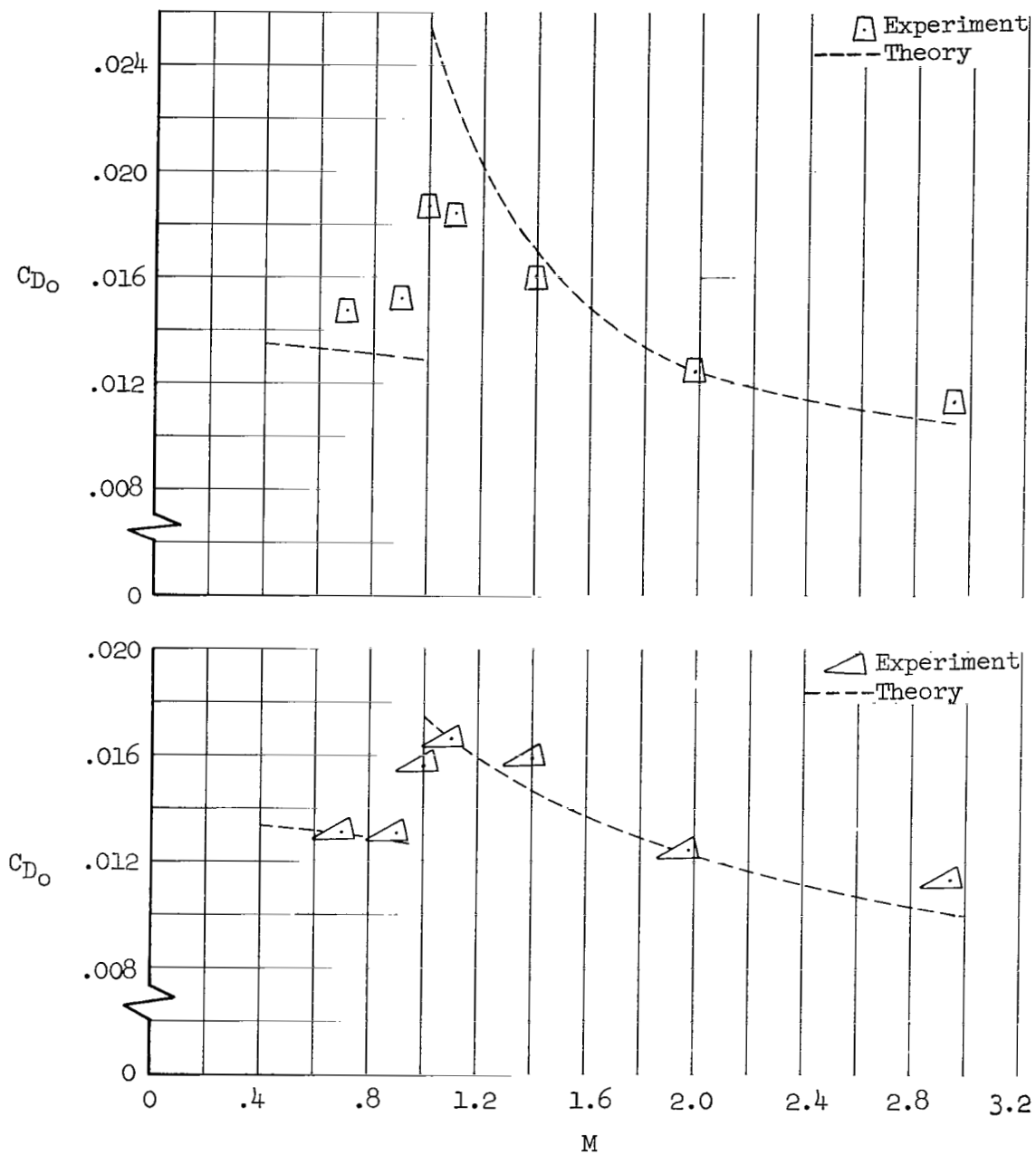

(b) Trapezoidal and triangular wings.

Figure 12.- Concluded.

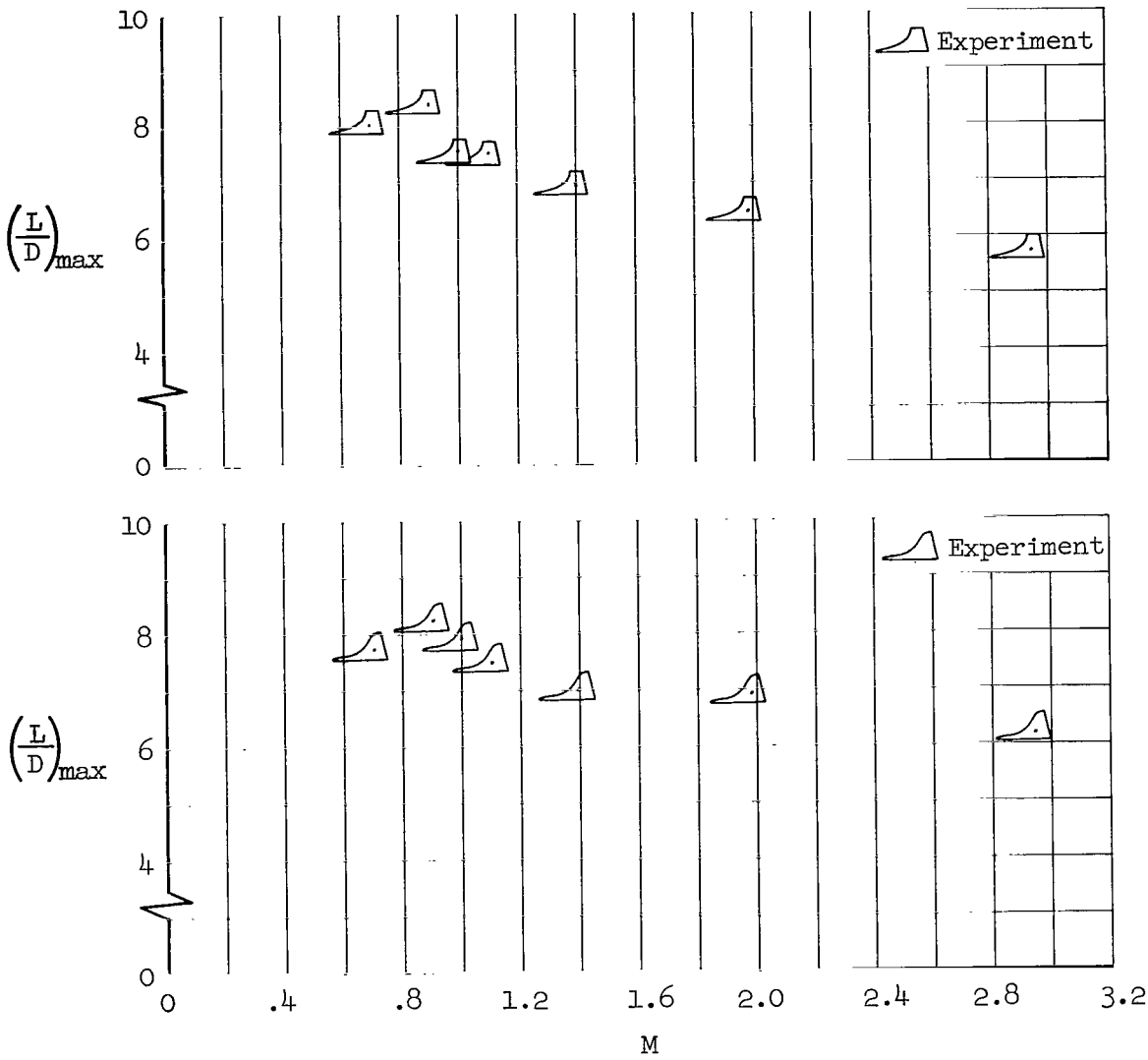

(a) Modified trapezoidal and ogee wings.

Figure 13.- Maximum lift-drag ratio as a function of Mach number.

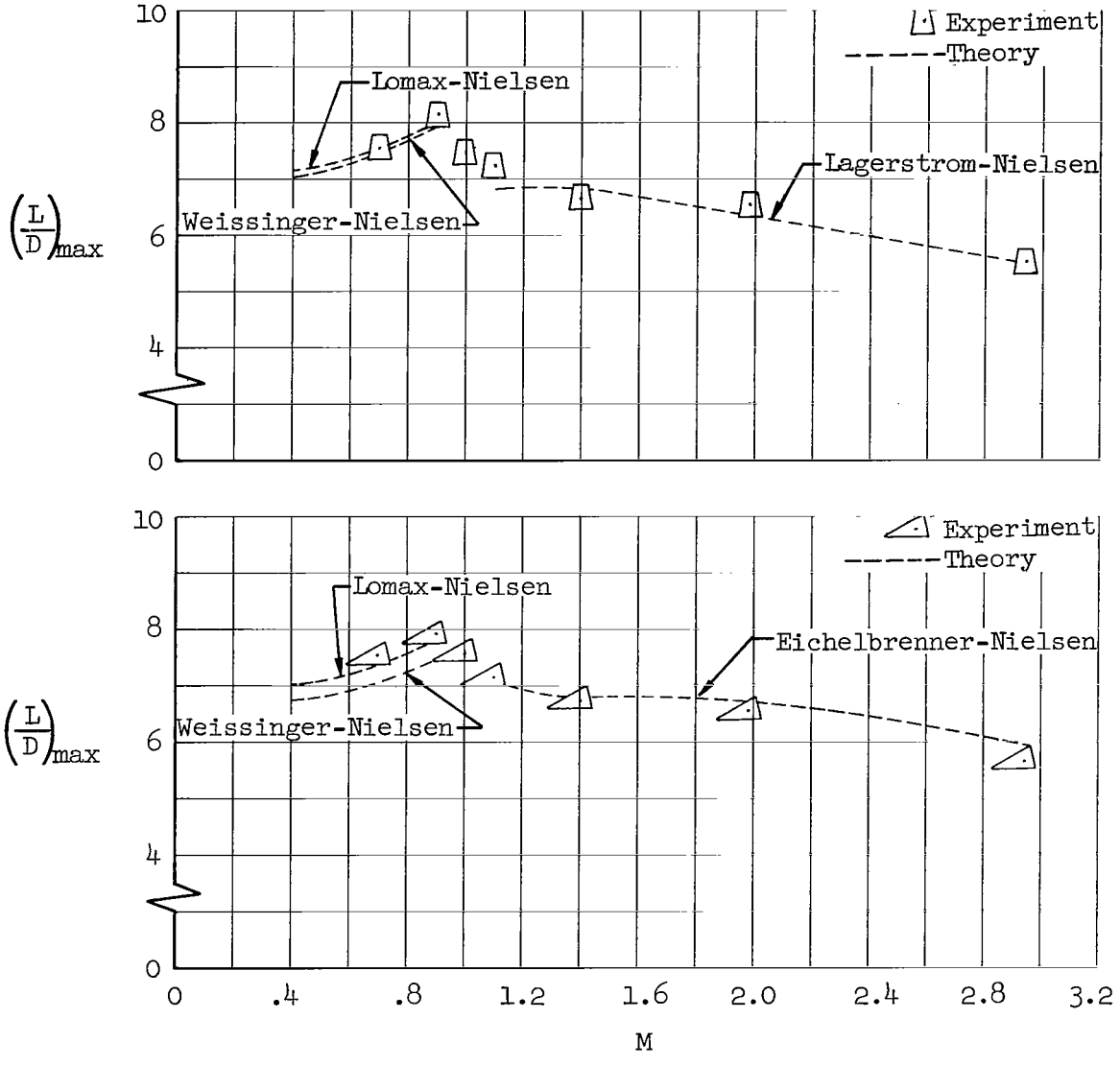

(b) Trapezoidal and triangular wings.

Figure 13.- Concluded.

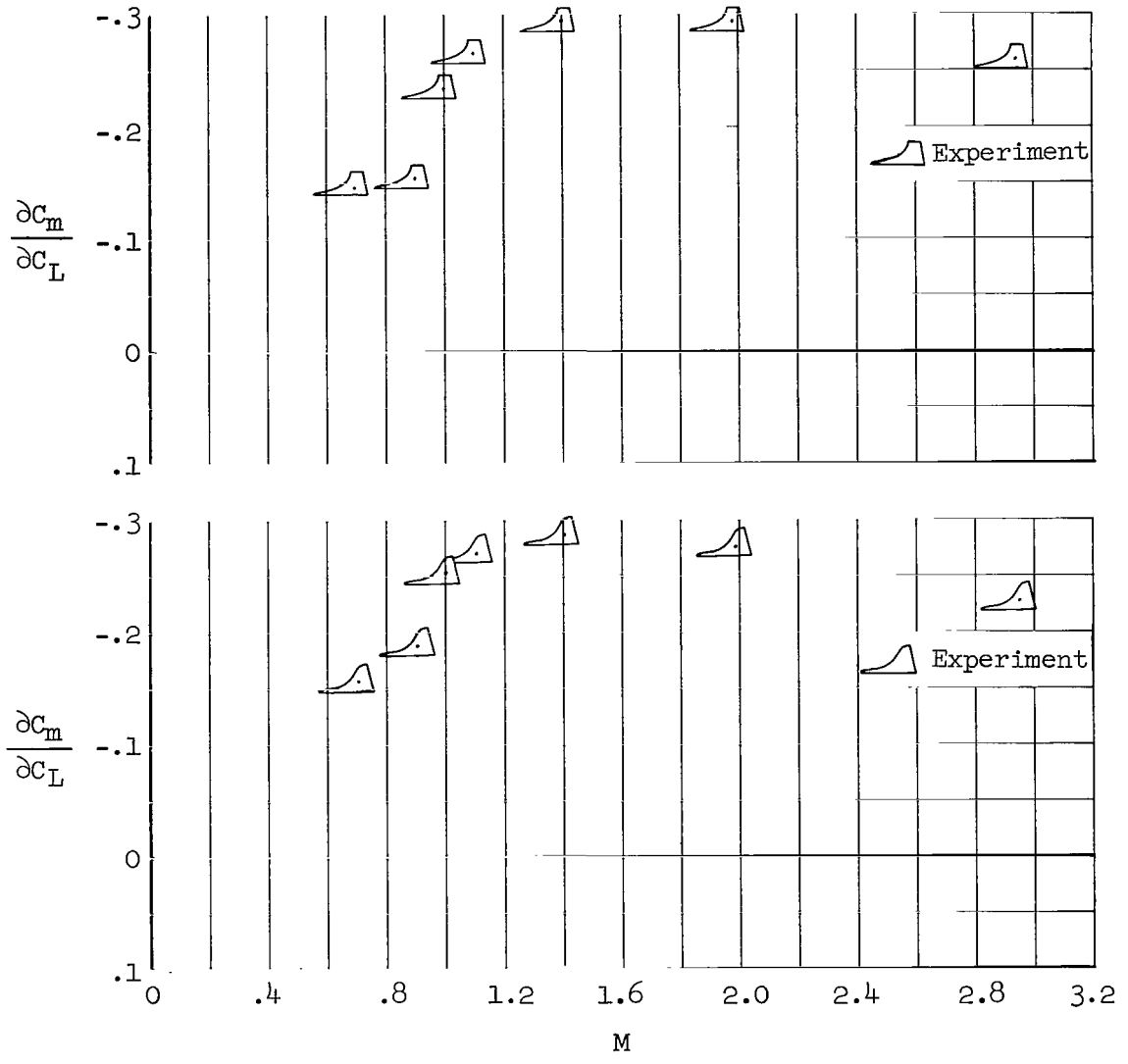

(a) Modified trapezoidal and ogee wings.

Figure 14.- Pitching-moment curve slope as a function of Mach number.

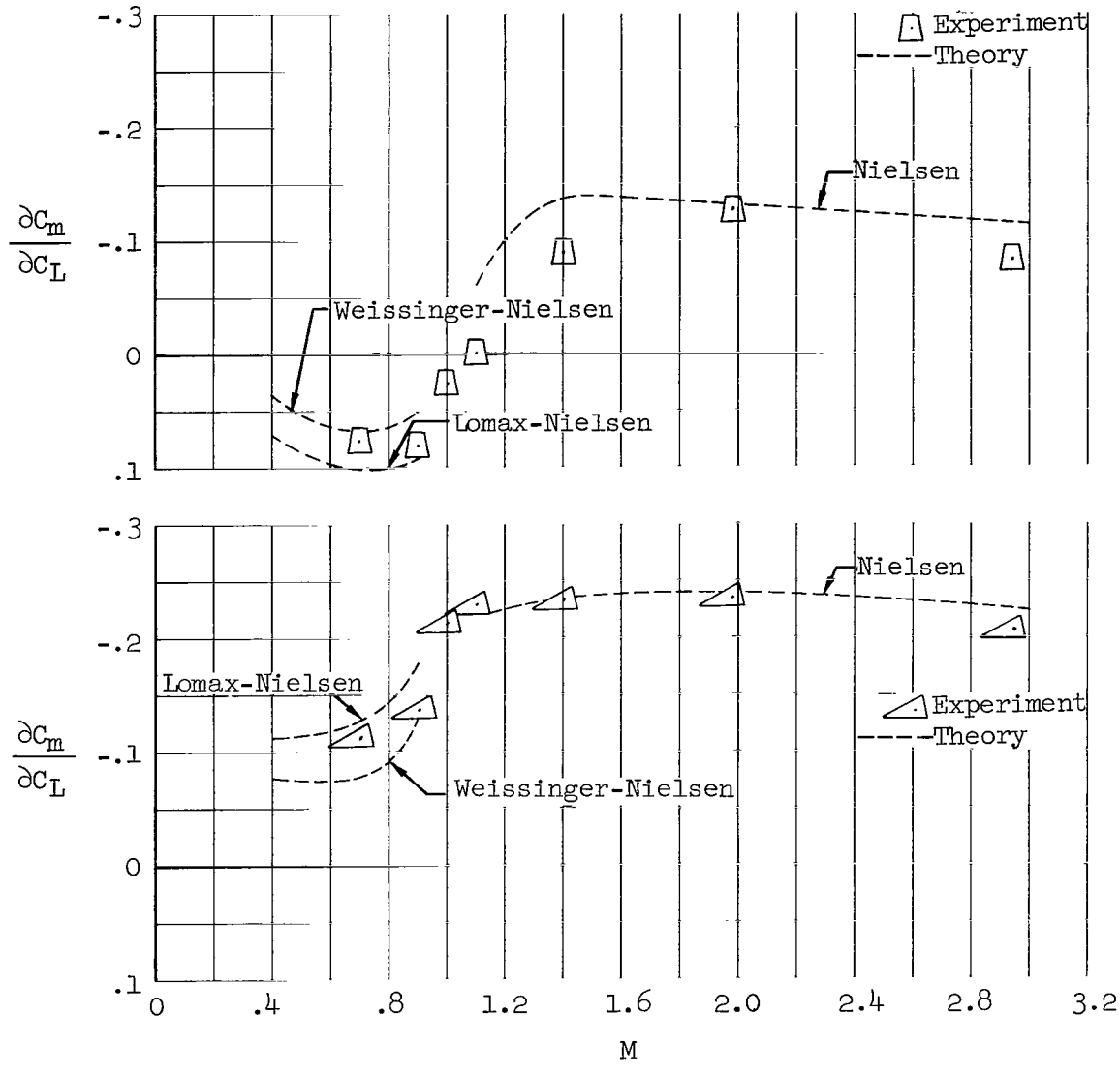

(b) Trapezoidal and triangular wings.

Figure 14.- Concluded.

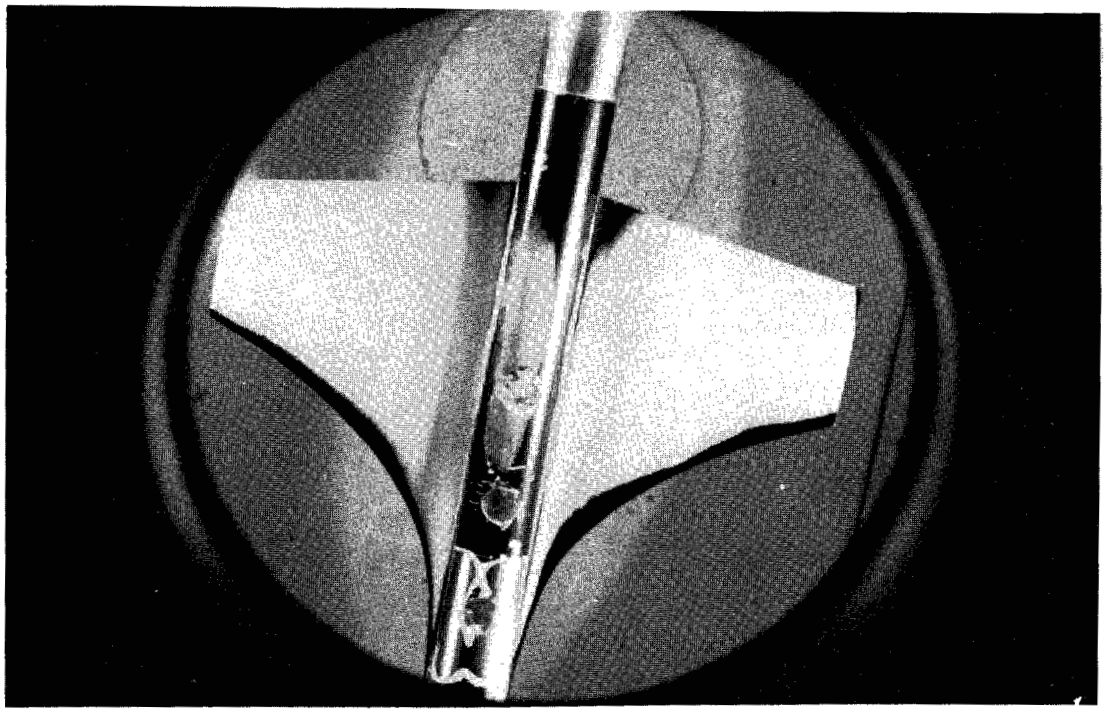

(a) $\alpha = 0^{\circ}$, upper surface.

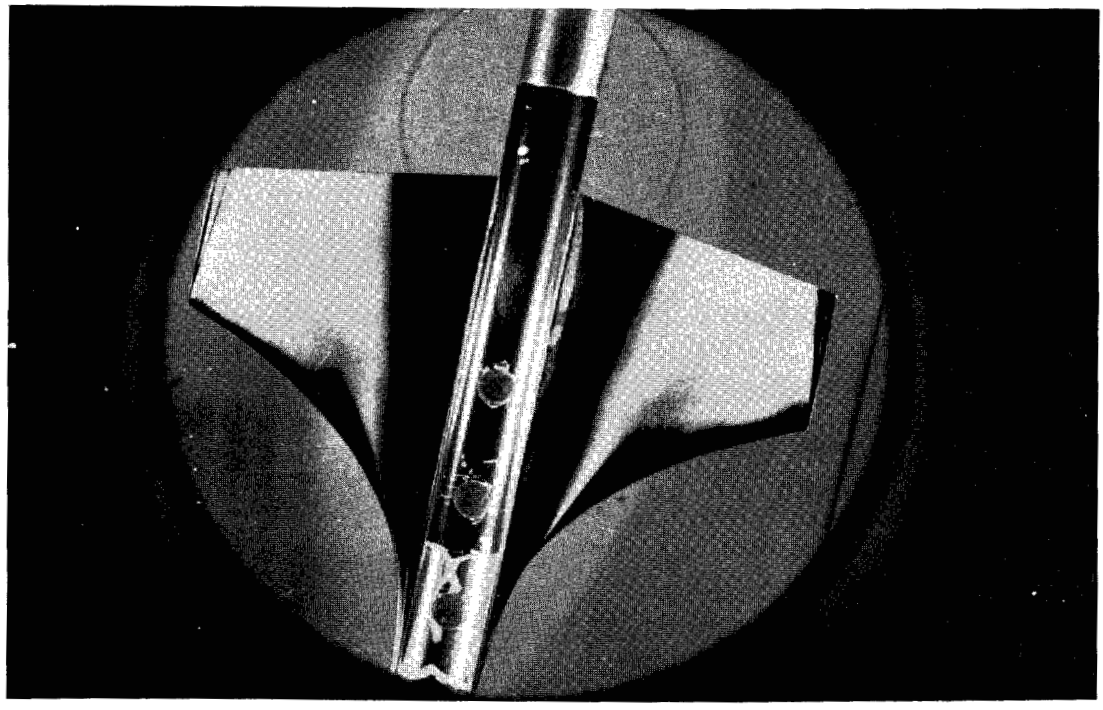

(b) $\alpha = 4^{\circ}$, upper surface.

Figure 15.- Typical sublimation photographs showing more laminar flow at $\alpha = 0^{\circ}$; M = 1.98.

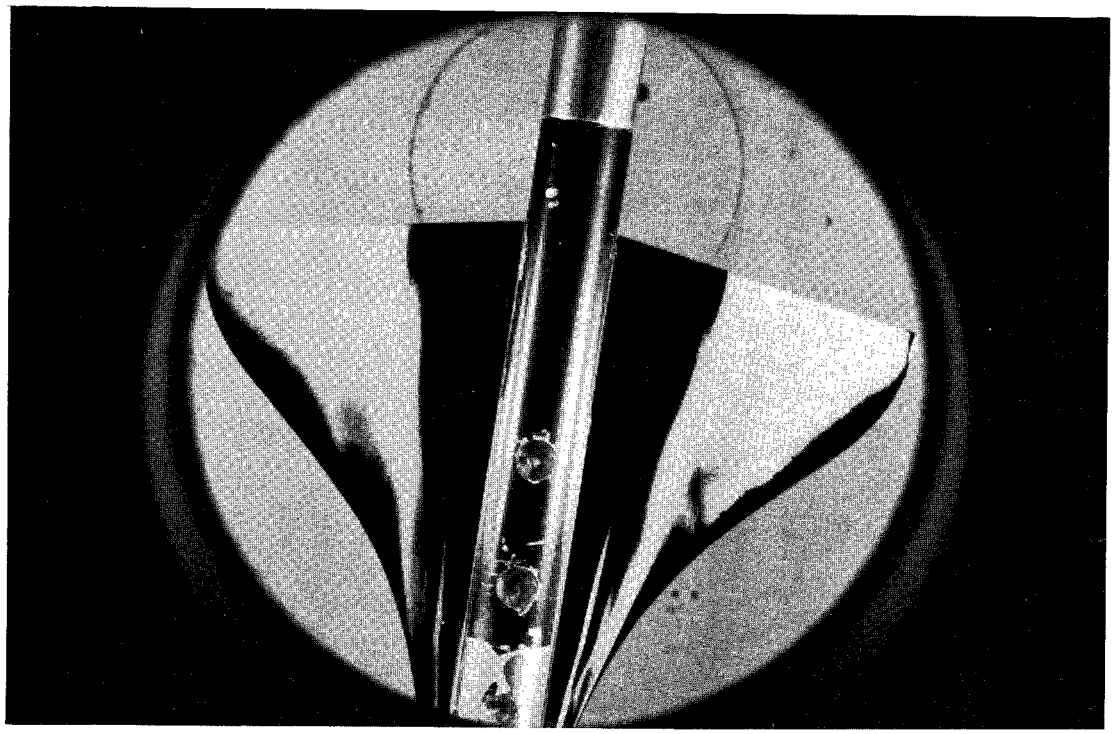

(a) Ogee wing, $\alpha = 4°$, upper surface.

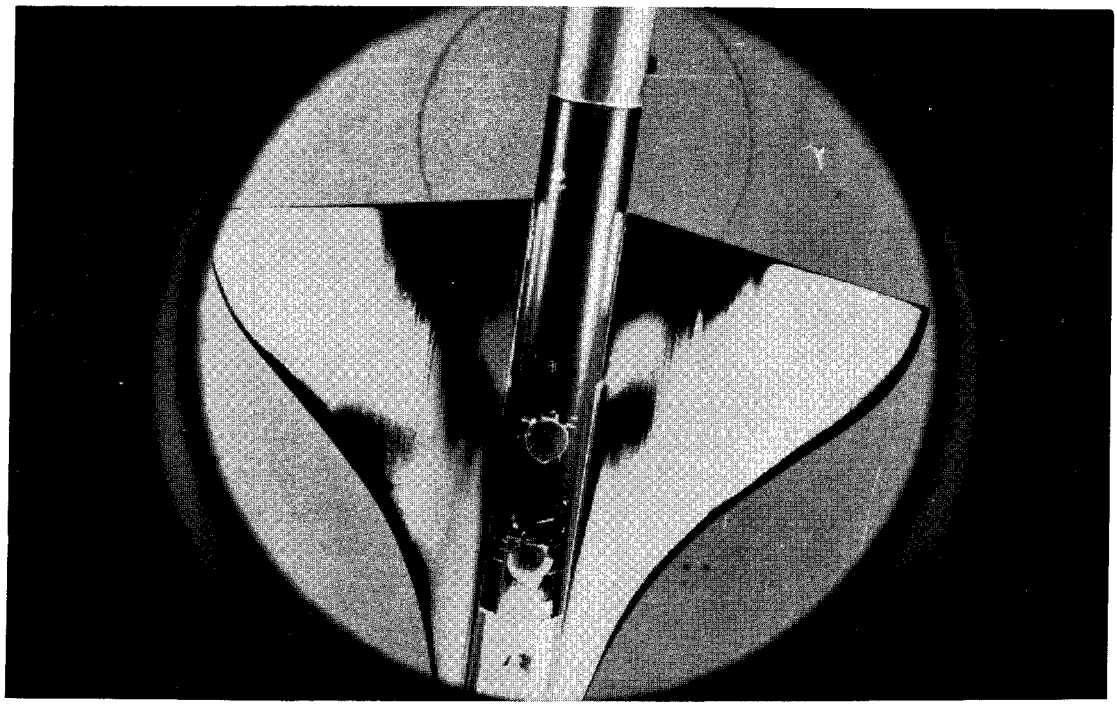

(b) Ogee wing, $\alpha = 4°$, lower surface.

Figure 16.- Typical sublimination photographs used in calculation of skin-friction coefficient; M = 2.94.

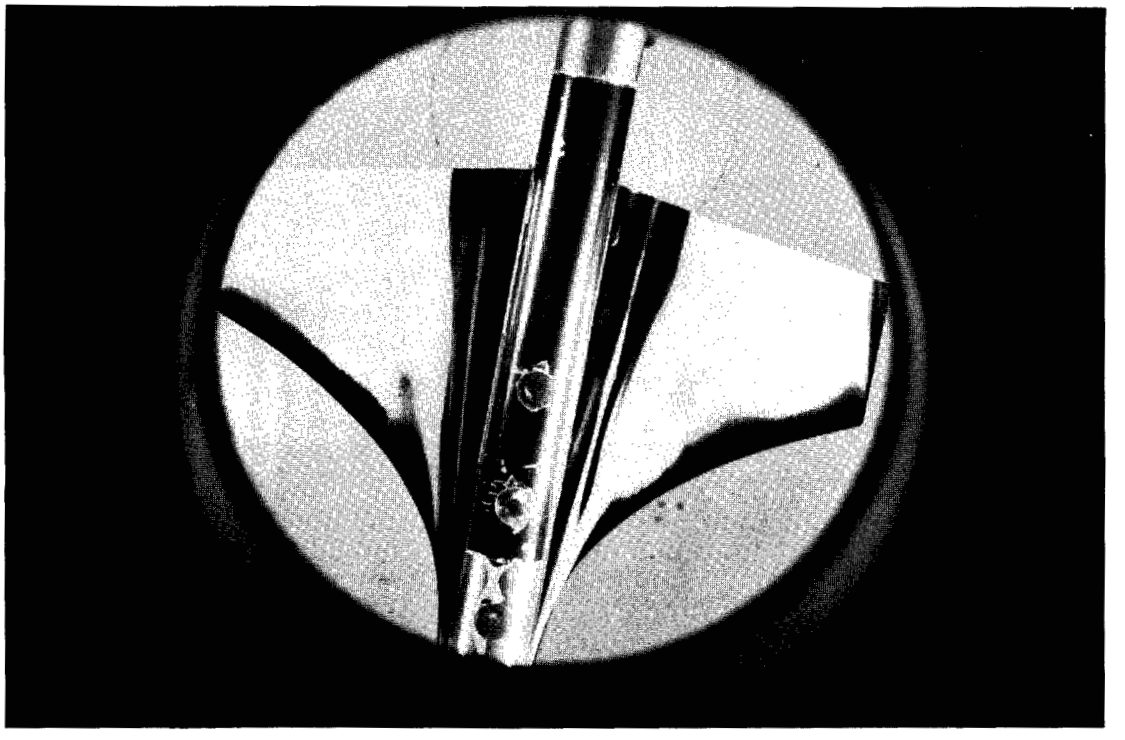

(c) Modified trapezoidal wing, $\alpha = 4°$, upper surface.

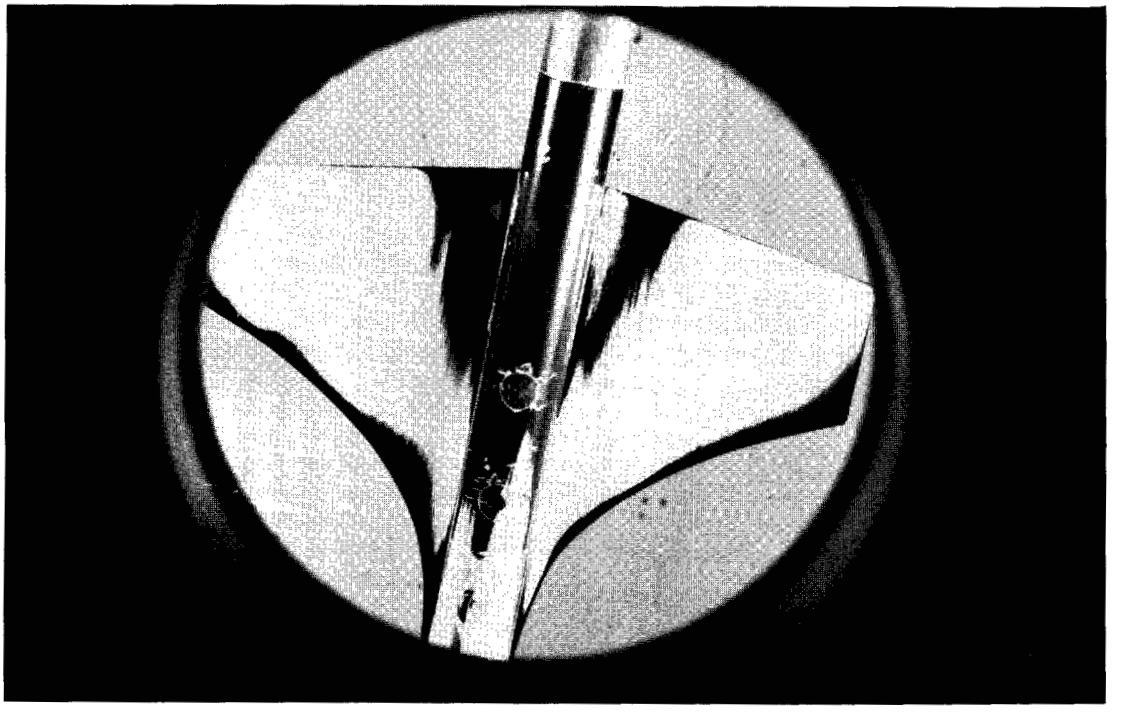

(d) Modified trapezoidal wing, $\alpha = 4°$, lower surface.

Figure 16.- Continued.

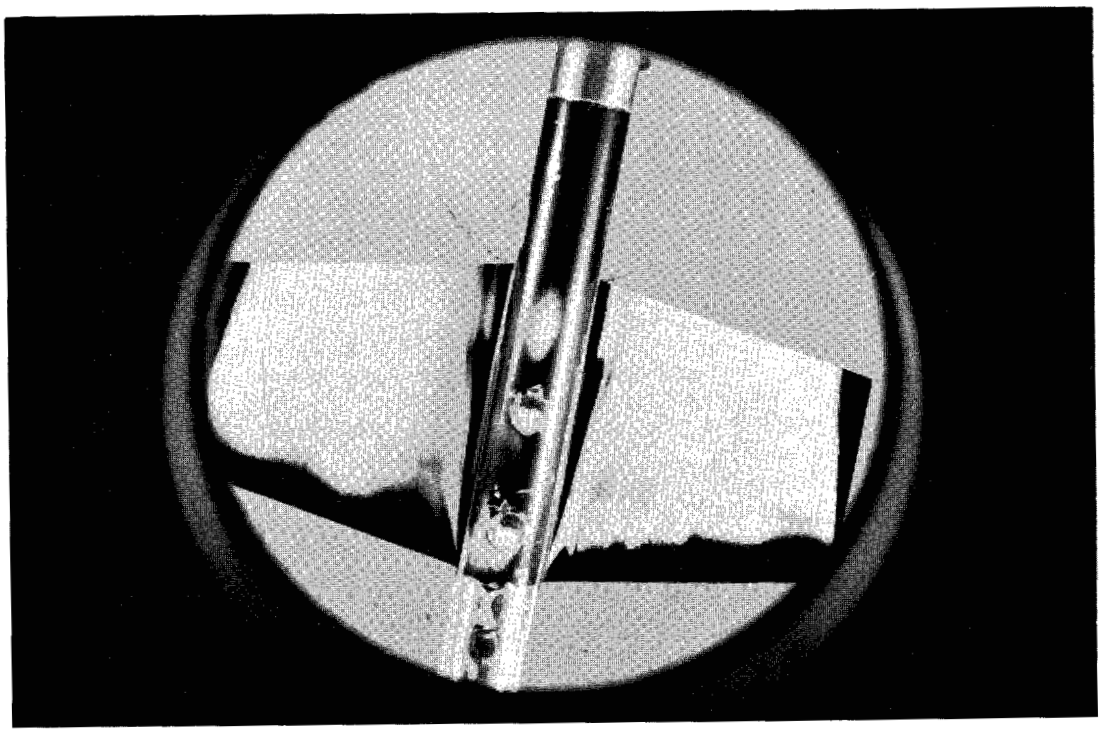

(e) Trapezoidal wing, $\alpha = 4°$, upper surface.

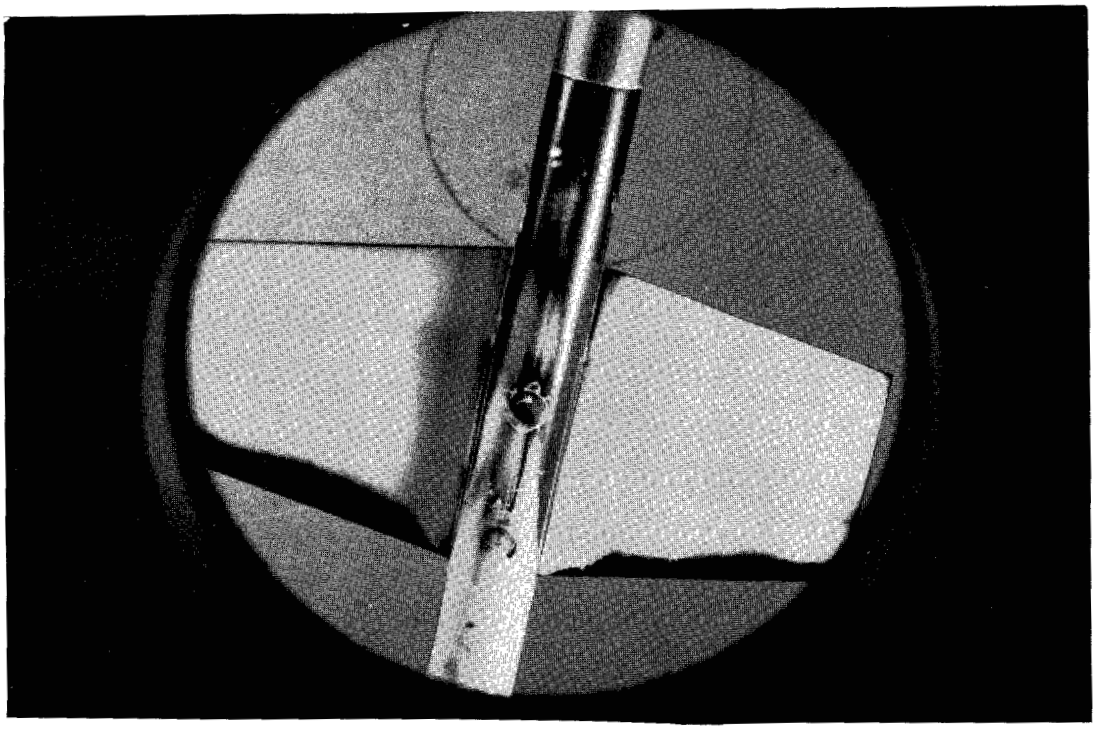

(f) Trapezoidal wing, $\alpha = 4°$, lower surface.

Figure 16.- Continued.

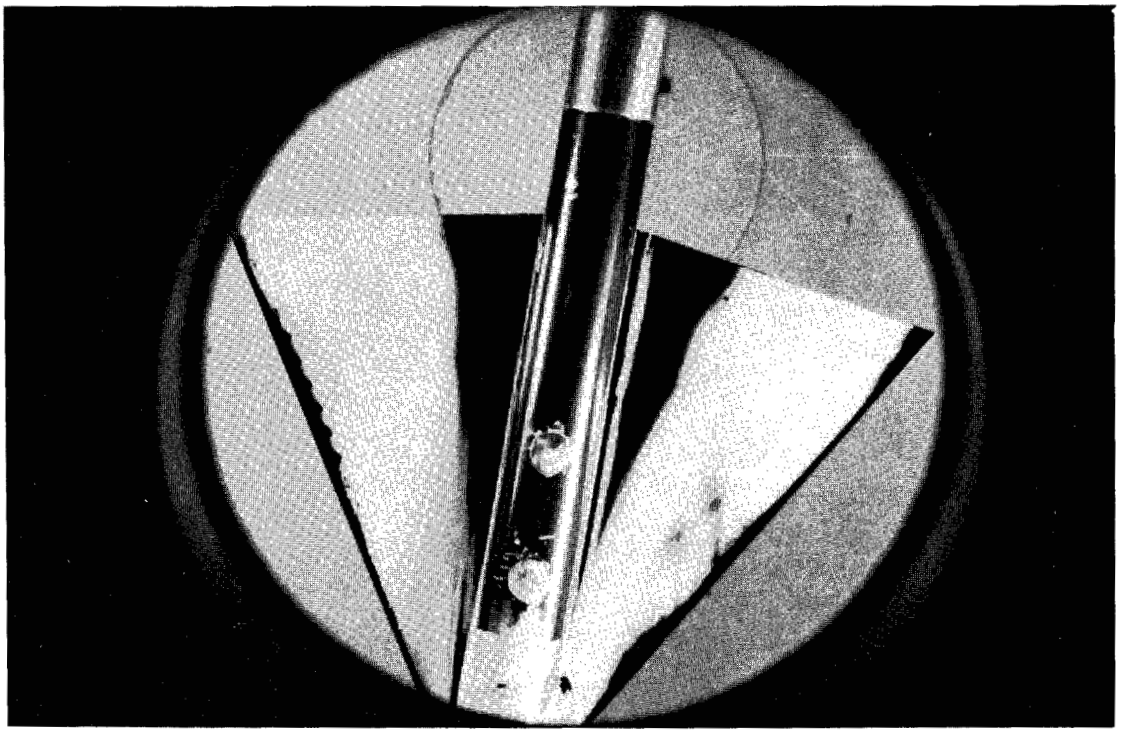

(g) Triangular wing, $\alpha = 4°$, upper surface.

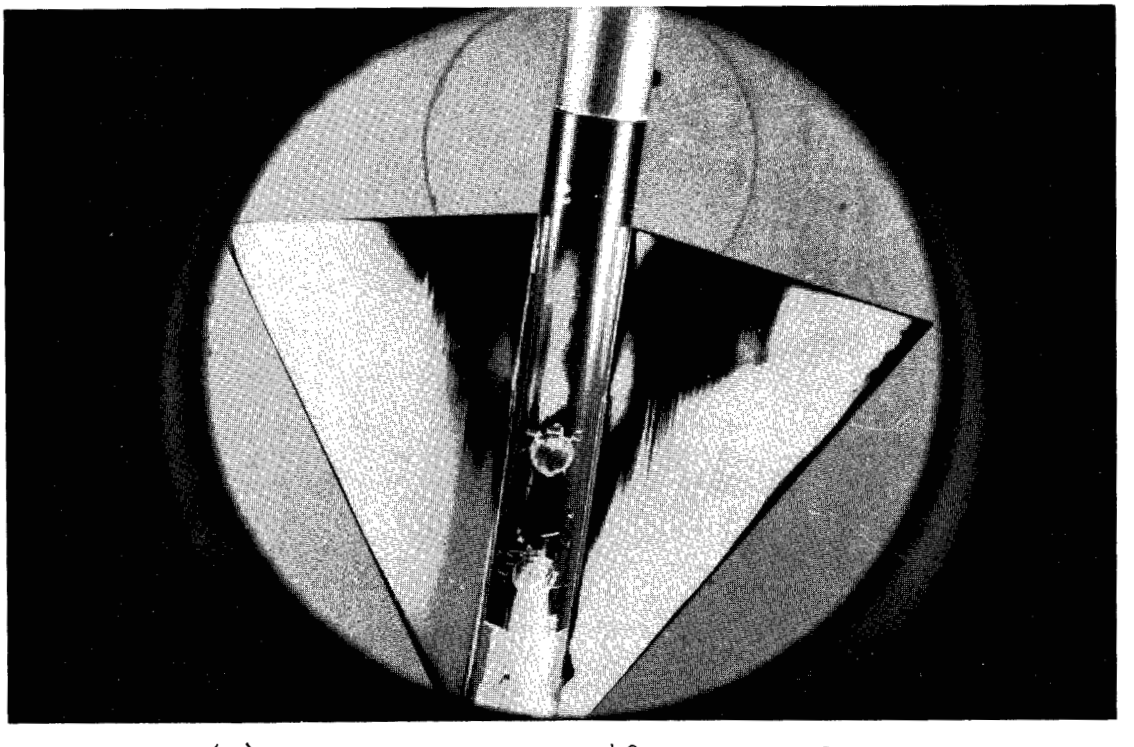

(h) Triangular wing, $\alpha = 4°$, lower surface.

Figure 16.- Concluded.

2/7/85

"The National Aeronautics and Space Administration . . . shall . . . provide for the widest practical appropriate dissemination of information concerning its activities and the results thereof . . . objectives being the expansion of human knowledge of phenomena in the atmosphere and space."

—National Aeronautics and Space Act of 1958

NASA SCIENTIFIC AND TECHNICAL PUBLICATIONS

TECHNICAL REPORTS: Scientific and technical information considered important, complete, and a lasting contribution to existing knowledge.

TECHNICAL NOTES: Information less broad in scope but nevertheless of importance as a contribution to existing knowledge.

TECHNICAL MEMORANDUMS: Information receiving limited distribution because of preliminary data, security classification, or other reasons.

CONTRACTOR REPORTS: Technical information generated in connection with a NASA contract or grant and released under NASA auspices.

TECHNICAL TRANSLATIONS: Information published in a foreign language considered to merit NASA distribution in English.

TECHNICAL REPRINTS: Information derived from NASA activities and initially published in the form of journal articles or meeting papers.

SPECIAL PUBLICATIONS: Information derived from or of value to NASA activities but not necessarily reporting the results of individual NASA-programmed scientific efforts. Publications include conference proceedings, monographs, data compilations, handbooks, sourcebooks, and special bibliographies.

Details on the availability of these publications may be obtained from:

SCIENTIFIC AND TECHNICAL INFORMATION DIVISION

NATIONAL AERONAUTICS AND SPACE ADMINISTRATION

Washington, D.C. 20546